PHYSICAL REVIEW C VOLUME 24, NUMBER 3 SEPTEMBER 1981

Structure of the giant multipole resonances in ^{20}Ne and ^{28}Si

K. W. Schmid

Institut für Theoretische Physik, Universität Tübingen, Auf der Morgenstelle 14, D-7400 Tübingen 1, Federal Republic of Germany

(Received 26 June 1980)

Nuclear structure wave functions for the ground and excited states of light deformed nuclei are obtained by diagonalizing a "realistic" many nucleon Hamiltonian (kinetic energy plus a Brueckner G matrix based on the Hamada-Johnston potential) in a suitably truncated nonorthogonal space of angular momentum projected deformed Slater determinants being constructed out of self-consistent Hartree-Fock single nucleon orbits. Possible spurious admixtures due to the center of mass motion are eliminated at least approximately by a separate diagonalization of the center of mass Hamiltonian. Taking into account a rather large single particle basis, calculations using this method are performed for the two sd-shell nuclei ^{20}Ne and ^{28}Si. Besides energies and wave functions, using alternatively an oscillator and a Woods-Saxon representation, the electromagnetic ground state transitions of both parities and of various multipolarities are also calculated as well as the corresponding spectroscopic amplitudes. The results are compared, where possible, with the experimental data and the results of other calculations. Special attention is paid to the strength distributions obtained for the various multipolarities. Though completely microscopic, the model yields fair qualitative agreement with the available experimental information. Furthermore, possible improvements of the method are discussed.

[NUCLEAR STRUCTURE ^{20}Ne, ^{28}Si; calculated level schemes and electromagnetic transitions. Angular momentum projected Hartree-Fock and particle-hole method. Structure of the giant multipole resonances.]

I. INTRODUCTION

Within the last few years the experimental information about the giant multipole resonances (GMR) in many nuclei has been rapidly accumulating.[1-4] While the electric giant dipole resonances ($E1V$) had already been studied extensively a long time ago, for example, by very accurate proton radiative capture experiments,[5-7] and while information about magnetic isovector dipole states ($M1V$) has also been available for more than a decade due to measurements of inelastic e scattering under backward angles,[8-10] it was mainly the access to high energy ^{4}He beams which opened a new field of investigation of the GMR's. Inelastic α-scattering experiments performed by various groups[4,11-18] did establish in the meantime the existence of an electric isoscalar giant quadrupole resonance ($E2S$) in many nuclei spread over the whole mass table. Furthermore, since in some nuclei even the decay of these $E2S$ states into various channels has been measured by coincidence experiments,[4,12,18] the isoscalar electric quadrupole mode of excitation today seems even better known than the famous $E1V$ resonances. Experiments searching for giant transition strengths of other multipolarities are going on. Though not yet completely conclusive, there is, for example, at least some experimental evidence for an electric isoscalar giant monopole state ($E0S$) in ^{208}Pb.[19] On the other hand, in nuclei below ^{40}Ca, up to now no energetically concentrated $E0S$ strength exhausting more than only a few percent of the corresponding classical energy weighted sumrule has been found.[20]

However, not only α-scattering experiments but also other ways to excite the various GMR's, for example inelastic proton scattering,[1] have increased our knowledge considerably. Refined inelastic electron scattering measurements have updated our information about the $M1V$ states.[21] Furthermore, the use of polarized proton beams opened new possibilities for the proton radiative capture measurements,[3,22] and last but not least even reactions with pions[23] and heavy ions[24] can be used as tools for the experimental study of the GMR's.

Naturally the enormous experimental progress on the GMR field was rather stimulating for the theoretical research on this problem. This holds especially true for the microscopic approaches to the structure of the GMR's. For doubly closed shell nuclei, within the last few years random-phase approximation (RPA) calculations in rather large model spaces have been performed,[25,26] and in some cases even the influence of two particle-two hole (2p2h) admixtures to the RPA wave functions have been taken into account, at least approximately, via the coupling of the RPA phonons to the low excited collective states of the nuclei considered.[27,28] It was shown that the higher order correlations explicitly included in this so called core-coupling RPA approach cause a large spreading of the GMR-transition strengths for most multipolarities and improve the agreement with the experimental findings considerably.

Furthermore, these calculations added much to our knowledge about effective particle-hole interactions, and last but not least, the transition densities calculated in this way which are being used as nuclear structure input for the analysis of inelastic electron, α, and proton scattering sucessfully reproduced many of the experimental data.[29]

In open shell nuclei, i.e., nuclei with a couple of nucleons outside the closed shells, the situation is more complex. While in doubly closed shell nuclei all the 1p1h—and even the 2p2h—excitations with respect to the spherical ground state can be easily coupled to definite total angular momentum, in open shell nuclei usually the Hartree-Fock (HF) vacuum, as well as the excitations with respect to it, break the required rotational symmetry. Therefore, in order to obtain physical states here, angular momentum projection techniques, which complicate the numerical calculations considerably, have to be applied. Further complications result from the fact that the angular momentum projected deformed 1p1h states do mix into the angular momentum projected HF vacuum, so that an RPA description of the excited states becomes invalid. Even restoring the required rotational symmetry before the variation of the HF degrees of freedom, which makes the resulting angular momentum projected HF vacuum stable against arbitrarily projected 1p1h admixtures, does not help, since then, as has been shown in Ref. 30, the particle orbits can no longer be defined in a physical way, and a description of the excited states then requires methods which are more complicated than a particle-hole expansion.

Knüpfer *et al.*[31] circumvented these problems by a sort of weak coupling approach. They tried to describe the GMR's in light deformed nuclei by coupling the RPA wave functions obtained for the GMR's in the spherical core ^{16}O to the valence wave functions obtained by the diagonalization of some effective Hamiltonian in an *sd*-shell model basis. The configuration mixing of these coupled states was then obtained by the diagonalization of a phenomenologically chosen, separable effective residual interaction. Obviously this approach has a couple of drawbacks. First, the wave functions are not antisymmetrized and hence violate the Pauli principle. Second, the polarization of the ^{16}O core by the *sd*-shell nucleons is only partly taken into account. Last but not least, the method requires the introduction of three different effective Hamiltonians, which have, in general, nothing to do with each other and therefore make the results somewhat ambiguous. Though being somewhat successful, Knüpfer's calculations can therefore only be considered as some semimicroscopic approach to the GMR's in the light deformed nuclei; this approach definitely has its merits but should obviously be improved on a more microscopic basis.

Such a microscopic theory is the angular momentum projected deformed particle hole model which has been developed in Refs. 32 and 33. In this approach the wave functions for the ground and excited states are approximated by linear combinations of the angular momentum projected deformed Hartree-Fock vacuum and the angular momentum projected 1p1h excitations with respect to it, and the configuration mixing coefficients of this expansion are obtained from the same total Hamiltonian also used for the calculation of the average HF field. In Ref. 33 these wave functions were then used as nuclear structure input for an also completely microscopic calculation of the proton radiation capture reaction. It was shown that in this way the structure of the GMR's in ^{20}Ne as seen via the (p,γ) reaction on ^{19}F could be reasonably well reproduced.

However, the (p,γ) reaction is a very selective process and tests only very specific parts of the total wave functions. Therefore, in the calculations presented in Ref. 33, only relatively small model spaces were needed and effective single particle energies and two body forces were used. For the analysis of more complex reactions like inelastic electron or hadron scattering the wave functions so obtained are obviously much too restricted.

In the present investigation the model will therefore be extended to rather large single particle spaces. This enables us to use a microscopic Brueckner *G* matrix and kinetic energy matrix elements such as the Hamiltonian to avoid the ambiguities connected with the introduction of effective single particle energies and interactions.

Section II will summarize the essential ingredients of this nuclear structure model. A detailed discussion of its application to the two nuclei ^{20}Ne and ^{28}Si will then be presented in Sec. III. The main results of the various calculations for these two nuclei with special emphasis on the GMR's are then discussed in Sec. IV, and Sec. V will finally summarize the essential points of the present investigation.

II. THEORY

Since the angular momentum projected deformed particle hole model (PHM) has already been described in detail elsewhere,[33] we shall give only a sort of summary of the main ideas this approach is based on and concentrate our discussion mainly

on the implications of the various approximations being introduced in its derivation.

We start as usual in conventional microscopic nuclear structure theory, defining a finite model space by an M dimensional, orthonormal set of single nucleon wave functions being discrete eigenstates of some spherical basis creating potential (for example, the harmonic oscillator or, if the continuum is discretized in a suitable way,[34] the Woods-Saxon one). The creation operators for these basis states are denoted by $\{C_a^+, C_b^+ \ldots\}_M$. We shall furthermore assume that the total effective many nucleon Hamiltonian appropriate for this model space is known and can be written in the chosen representation as a sum of only one and two body terms

$$\hat{H} = \sum_{ab} t(ab) C_a^+ C_b + \tfrac{1}{4} \sum_{abcd} v(acbd) C_a^+ C_c^+ C_d C_b \,. \quad (1)$$

Here $t(ab) := \langle a | \hat{t} | b \rangle$ are the matrix elements of the kinetic energy operator (or, if an inert core is assumed, some spherical single particle energies), and $v(acbd) := \langle ac | \hat{V} | bd - db \rangle$ denote the antisymmetrized two body matrix elements of the effective nucleon-nucleon interaction (for example, a Brueckner G matrix such as that of Ref. 35 or some more phenomenological potential such as the Skyrme force[36] or others).

The straightforward way to obtain the A-nucleon eigenstates of (1) would then be to diagonalize this Hamiltonian in the space of all the A-nucleon Slater determinants, which can be constructed in the chosen model space, and each of which describes the independent motion of the particles in the field of the basis creating potential. Unfortunately, this "shell model configuration mixing" (SCM) approach[37,38] is limited to rather small model spaces for numerical reasons and hence cannot be applied to the highly excited states in the region of the GMR's. Being interested in these states one has therefore to develop a truncation scheme which reduces the dimension of the configuration space to manageable size without eliminating those degrees of freedom which are essential for the particular nuclear excitations under investigation.

For this purpose first an HF calculation[39,40] for the considered nucleus is usually performed. This procedure extracts the average field each of the nucleons feels due to its interactions with all the others directly from the total Hamiltonian (1). The resulting HF vacuum, i.e., that Slater determinant in which the A energetically lowest orbits of this average potential are occupied ("hole" states) and all the other $(M-A)$ ones are empty ("particle" states), represents the optimal independent particle approach to the ground state of the considered system within the chosen model space.

Mathematically, the HF field is given by a unitary transformation of the single nucleon basis wave functions

$$a_i^+ = \sum_{a=1}^{M} A_{ai} C_a^+ \quad (i = 1, \ldots, M) \quad (2)$$

with

$$\sum_{a=1}^{M} A_{ai}^* A_{ak} = \delta(i,k) \quad (i,k = 1, \ldots, M) \,. \quad (3)$$

The HF Slater determinant can then be written as

$$|\rangle = \prod_{i \le F}^{(A)} a_i^+ |0\rangle \,, \quad (4)$$

where $|0\rangle$ denotes the particle vacuum and the product runs over the A energetically lowest orbits (2) of the self-consistent HF potential up to some Fermi level F. The transformation matrix in Eq. (2) is then determined by a variational principle requiring a minimum for the expectation value of the total Hamiltonian (1) in the test wave function (4) with respect to variations of the expansion coefficients A_{ai} in Eq. (2) and being subject to the unitarity constraint (3).

Any virtual or real excitation of the system can then be represented in terms of particle-hole (ph) excitations with respect to the reference determinant (4). Besides the configuration (4), the total configuration space in the HF representation consists of the 1p1h excitations with respect to it

$$|\alpha^{-1} L\rangle = a_L^+ a_\alpha |\rangle \quad (\alpha \le F; L > F) \,, \quad (5)$$

the 2p2h configurations, and so on, up to the $Ap Ah$ terms.

Obviously, if all these configurations really had to be taken into account we would have gained nothing with respect to the SCM approach. However, while the SCM configurations are defined with respect to an arbitrary, *ad hoc* chosen potential, the HF method obtains the best possible reference field and minimizes the residual interactions, at least for the ground state of the nucleus. One can therefore hope that an expansion of the nuclear wave functions in terms of ph configurations with respect to the HF vacuum (4), even if already truncated after the 2p2h or even after the 1p1h terms, may still be a reasonable approximation to the exact SCM solutions for many states of the considered system.

In the convential Tamm-Dancoff approximation (TDA) or the more sophisticated RPA, which has been applied with great success to the GMR problem in doubly closed shell nuclei,[25,26] use is made of the fact that the Hamiltonian (1) does not connect the 1p1h excitations (5) with the refer-

ence state (4) because of Thouless's theorem.[41] In first approximation the ground state of the nucleus may therefore be represented by the latter and the excited states be obtained by diagonalizing the Hamiltonian (1) only in the 1p1h space (5). Since the electromagnetic transition operator has only one body terms, the resulting states, at least in the RPA approach which takes into account at least implicitly some of the ground state correlations neglected in (4), do exhaust the full energy weighted sumrule strengths for the various multipole transitions, and only if the intermediate and fine structure of the spectra is considered, also the coupling of the RPA states to higher order correlations; for example, the 2p2h configurations, have to be taken into account. If this is done, the spreading of the GMR strengths over many states, which is experimentally observed even in spherical nuclei like ^{16}O and ^{208}Pb, can also be reasonably well described.[27,28]

However, while in spherical nuclei all the configurations (5) and even the higher order ones can be easily coupled to definite angular momentum, in open shell nuclei (i.e., nuclei with a couple of nucleons outside the closed shells) the situation is more complex. Here, in general, the HF reference determinant (4) as well as the ph excitations with respect to it, are deformed. Being neither eigenstates of the square of the total angular momentum operator $\hat{I}^2$ nor of its projection $\hat{I}_z$ on the z axis of the laboratory frame, these states cannot be considered physical states but only some intrinsic structure from which the physical components with the required rotational symmetry still have to be obtained, for example, by angular momentum projection methods.

The technique of projecting the components with good total spin I and spin projection M on the lab z axis from an arbitrary antisymmetrized A-nucleon wave function has been well known for a long time[42,43] and has only recently been the subject of some review papers.[44] We shall therefore give here only a short summary of this method.

Let $\{\phi_c; c=1,\ldots,N\}$ be a set of (not necessarily orthogonal) deformed Slater determinants, for example of the types (4) and (5). Each of these determinants can obviously be expanded in terms of a complete, orthonormal set of A-nucleon states being eigenfunctions to $\hat{I}^2$ and its projection $\hat{I}_3$ on the intrinsic 3 axis with eigenvalues $I(I+1)\hbar^2$ and $K\hbar$, respectively. Denoting by ν the additional quantum numbers required to distinguish between the different states with the same I and K we may write

$$|\phi_c\rangle=\sum_{IK\nu}|IK\nu\rangle\langle IK\nu|\phi_c\rangle . \tag{6}$$

Villars's angular momentum projection operator[43]

$$\hat{P}(IM;K)=\sum_{\nu}|IM\nu\rangle\langle IK\nu| \tag{7}$$

applied on (6) then creates a set of nonorthogonal and unnormalized configurations

$$|\phi_cK;IM\rangle=\hat{P}(IM;K)|\phi_c\rangle=\sum_{\nu}|IM\nu\rangle\langle IK\nu|\phi_c\rangle , \tag{8}$$

which are now eigenfunctions of $\hat{I}^2$ and its projection $\hat{I}_z$ on the lab z axis with eigenvalues $I(I+1)\hbar^2$ and $M\hbar$, respectively. Note that the operator (7) is a projector in its strict mathematical sense only for $M=K$. Its nondiagonality in these indices takes into account that states with the same M may be obtained from all the different components with intrinsic spin projections $|K|\leq I$ contained in the deformed wave function (6). Therefore the configurations (8) still depend on the orientation of the intrinsic system [rotating (6) changes the K distribution] and hence cannot yet be considered a physical basis. Orientation independent wave functions can, however, easily be obtained by taking general linear combinations of the nonorthogonal configurations (8).

The most general symmetry conserving test wave function constructable from the deformed set (8) then has the form

$$|IM;d\rangle=\sum_{cK}|\phi_cK;IM\rangle f^{(I)}_{cK;d} , \tag{9}$$

where d enumerates the different possible states with the same angular momentum quantum numbers and the expansion coefficients $f^{(I)}_{cK;d}$ can be easily obtained by requiring a minimum of the energy expectation value within the test wave function (9). This yields a matrix equation

$$\sum_{c'K'}\{\langle\phi_cK;IM|\hat{H}|\phi_{c'}K';IM\rangle - E_d(I)\langle\phi_cK;IM|\phi_{c'}K';IM\rangle\}f^{(I)}_{c'K';d}=0 , \tag{10}$$

where the orthogonality of the resulting wave functions (9) is ensured by the additional constraint

$$\sum_{cKc'K'}f^{*(I)}_{cK;d}\langle\phi_cK;IM|\phi_{c'}K';IM\rangle f^{(I)}_{c'K';d'}=\delta(d,d') . \tag{11}$$

The system of equations (10) and (11) solves our problem of restoring the required rotational symmetry. Since here the angular momentum projection is performed before the variation of the configuration mixing degrees of freedom $f^{(I)}_{cK;d}$, the equations determine separately for each spin the optimal linear combination of the wave functions (6), and hence the dynamic spin dependence of the various degrees of freedom is automatically taken

into account. Furthermore, the overlap matrix in Eqs. (10) and (11) takes care of the possible linear dependencies in the nonorthogonal set of configurations (8).

In general, since the expansion (6) is usually not known, the energy and overlap matrices in the above equations cannot be calculated from the general expression (8). However, it can be easily shown that the projection operator (7) can be represented as an integral operator

$$\hat{P}(IM;K)=\frac{2I+1}{8\pi^2}\int d\Omega D^{I*}_{MK}(\Omega)\hat{R}(\Omega)\,, \tag{12}$$

where Ω denotes the three Euler angles, $\hat{R}(\Omega)$ is the usual rotation operator,[45] and $D^I_{MK}(\Omega)$ its representation in angular momentum eigenfunctions. Using (12) instead of (7) the overlap and energy matrices in Eqs. (10) and (11) can be written as

$$N^{(I)}_{cK;c'K'}=\langle\phi_c K;IM\,|\,\phi_{c'}K';IM\rangle$$

$$=\frac{2I+1}{8\pi^2}\int d\Omega D^{I*}_{KK'}(\Omega)\langle\phi_c|\hat{R}(\Omega)|\,\phi_{c'}\rangle \tag{13}$$

and

$$H^{(I)}_{cK;c'K'}=\langle\phi_c K;IM\,|\hat{H}|\,\phi_{c'}K';IM\rangle$$

$$=\frac{2I+1}{8\pi^2}\int d\Omega D^{I*}_{KK'}(\Omega)\langle\phi_c|\hat{H}\hat{R}(\Omega)|\,\phi_{c'}\rangle \tag{14}$$

and hence can be evaluated without knowing the expansion (6) explicitly.

Obviously, if no symmetry restrictions are imposed on the HF expansion (2) the calculation of the overlap and energy matrices (13) and (14) becomes rather involved numerically because of the threefold integrations induced by the projection operator (12). In order to simplify our problem we shall therefore restrict ourselves in the following to doubly even nuclei with an equal number of protons and neutrons, neglect the Coulomb repulsion between the protons, and forbid parity mixing in the HF transformation (2). Furthermore, we shall impose axial symmetry on the HF orbits and truncate the configuration space after the 1p1h terms (5).

Because of these approximations, parity, isospin projection, and spin projection on the internal 3 axis can be considered "good" quantum numbers in the expansion (2). Furthermore, proton and neutron states with the same quantum numbers are degenerate, as is each of the self-consistent orbits $|i\rangle$ from Eq. (2) with its time reversed partner

$$|\bar{i}\rangle=\mathcal{T}a^+_i|\,0\rangle=\sum_a A_{ai}(-)^{l_a+j_a-m_a}C^+_{a(-m_a)}|\,0\rangle\,. \tag{15}$$

Consequently, the HF determinant (4) has total isospin and isospin projection $T=T_z=0$, intrinsic spin projection $K=0$, positive parity $\pi=+$, and is even under time reversal. Applying the projection operator (12) on this state we therefore obtain the configuration

$$|\,0;I^\pi MT(T_z=0)\rangle=\delta(\pi,+)\delta(T,0)\delta((-)^I,+)\hat{P}(IM;0)|\,\rangle\,. \tag{16}$$

Furthermore, the 1p1h configurations (5) also have definite parity ($\pi=\pi_\alpha\cdot\pi_L$) and intrinsic spin projections ($K=m_L-m_\alpha$) and can be easily coupled to total isospin T and isospin projection $T_z=0$. Also using the time reversal properties of (5) here we obtain, by applying the projection operator (12),

$$\begin{aligned}|\,\alpha^{-1}L;I^\pi MT(T_z=0)\rangle=\delta(\pi_\alpha\cdot\pi_L,\pi)\delta(|m_L-m_\alpha|\le I)\delta(m_L>0)\\ \times\tfrac{1}{2}\{\hat{P}(IM;m_L-m_\alpha)[a^+_{L_p}a_{\alpha_p}+(-)^T a^+_{L_n}a_{\alpha_n}]|\,\rangle\\ +\pi(-)^{I-(m_L-m_\alpha)}\hat{P}(IM;-m_L+m_\alpha)[a^+_{L_p}a_{\bar{\alpha}_p}+(-)^T a^+_{L_n}a_{\bar{\alpha}_n}]|\,\rangle\}\,,\end{aligned} \tag{17}$$

where T may adopt the value 0 or 1, the subindices p and n indicate whether a proton or a neutron orbit is meant, and the bars denote the time reversed orbits according to our definition (15).

Since all the Slater determinants involved here have definite K values, the calculation of the overlap and energy matrices (13) and (14) within the nonorthogonal configuration space (16) and (17) is very much simplified. The integrations over two of the three Euler angles can be performed analytically and one is left with only one numerical integration. Solving the matrix equation (10) we obtain then the PHM wave functions

$$\begin{aligned}|I^\pi MT(T_z=0);d\rangle=|\,0;I^\pi MT(T_z=0)\rangle f_{0;d}(I^\pi T)\\ +\sum_{\substack{\alpha\le F\\ L>F}}|\,\alpha^{-1}L;I^\pi MT(T_z=0)\rangle f_{\alpha L;d}(I^\pi T)\,,\end{aligned} \tag{18}$$

which will be used in the following for the description of the ground as well as of the excited states in light deformed doubly even $N=Z$ nuclei.

It is easily seen from the structure of the energy matrix $H(I^\pi T)$ in Eq. (14) that, since the Hamiltonian (1) contains only one and two body terms, the wave functions (18) take into account at most

3p3h correlations with respect to the intrinsic HF reference state (4). Up to this limit, however, the system can choose rather complicated linear combinations of Slater determinants, if these are energetically favored, since the angular momentum projection is performed before the diagonalization of the Hamiltonian. Obviously this freedom is somewhat restricted by the properties of the projection operator (12). Therefore only a fraction of the total 2p2h and 3p3h degrees of freedom is really accessible. The magnitude of this fraction depends on the size of the model space and decreases with the increasing dimension of the latter. However, at least part of the 2p2h and 3p3h correlations with respect to the HF vacuum (4) is implicitly taken into account here.

This is also the reason that in the PHM wave functions (18) the projected 1p1h configurations (17) do mix with the projected reference state (16), while such a mixing does not occur in the intrinsic configuration spaces (4) and (5) due to Thouless's theorem.[41] If the angular momentum projection had been performed not only before the variation of the configuration mixing but also of the HF degrees of freedom (2), this mixing would obviously vanish, and the projected reference determinant (16) would then be stable against arbitrary projected 1p1h admixtures of the type (17). However, it has been shown in Ref. 30 that in this case the particle states cannot be defined in a physical way and the excited states therefore have to be described in a rather different approach than by the expansions (4) and (5), which are meaningless in the case of ambiguous particle orbits. For the highly excited states in the GMR region, however, the approach presented here seems far more suitable; even more suitable if one considers that at least part of the spin dependent renormalization effects induced on the HF field by a spin projection before the variation of the single particle degrees of freedom is explicitly taken into account also by the wave functions (18) in terms of the mixing between the configurations (16) and (17). Note furthermore, that, though the intrinsic configurations (4) and (5) have all definite spin projections K, the total wave functions (18) do mix all the configurations with $|K| \leq I$, so that the intrinsic structure behind (18) can have rather general deformations.

Obviously, as soon as more than one major oscillator shell is taken into account in the model space, one is faced with the possible occurrence of spurious admixtures in the wave functions (18) due to the center of mass motion. This problem has been known for a long time[46,47] and will be treated in our approach in the following way. Instead of solving the matrix equation (10) directly for the total Hamiltonian (1), we first obtain its solutions for the center of mass Hamiltonian $H_{\text{c.m.}}$, which also contains only one and two body terms and can hence be handled in the same way as the original Hamiltonian (1). In the case that our configuration space were then complete with respect to the center of mass motions, we would then get a large number of eigenfunctions of the type (18) having all the same energy eigenvalue corresponding to the zero point energy of the center of mass motion, and (depending on parity, spin, and isospin) a few additional states, which are located at center of mass excitation energies of $1\hbar\omega$, $2\hbar\omega$, ... and have hence to be considered as spurious. The latter could then easily be projected out from the spectrum of the original Hamiltonian. Even if the configuration space is not complete, and this is usually the case, the above method[47] can still be used. Instead of having degenerate eigenvalues the center of mass eigenstates obtained from Eq. (10) are then clustered around the values given above, and, with a suitably chosen energy window, spurious and nonspurious states can still be separated and the latter can be removed from the spectrum of our many nucleon Hamiltonian (1). Such an at least approximate elimination of the spurious center of mass effects can be achieved.

Finally, I would like to draw your attention to a systematic drawback of the above described PHM configuration mixing approach. The intrinisc HF procedure used here to derive the reference field is specifically designed for the ground state of the nucleus. There is no *a priori* reason why the 1p1h configurations with respect to the same field should give equally good results for the highly excited states in the GMR region. In fact, the larger the model space and therefore the better the HF approach for the ground state, the larger the so called HF gap separating the particle from the hole orbits becomes. Hence one expects that the 1p1h configurations will be located at increasing excitation energy with respect to the ground state if the model space is increased. On the other hand, the strong contributions of, for example, the collective $2\hbar\omega$ excitations on the ground state band, which have been studied explicitly in Ref. 48, and are here to a large extent already taken into account by the average field via the inclusion of major shell mixing in the expansion (2), are also expected to have considerable effects on the excited states of the system. Microscopically, these renormalization effects could only be taken into account by including at least part of the 2p2h (or even higher order) correlations explicitly in the intrinsic configuration space. However, at least at present, such an extension of the config-

uration spaces (4) and (5) can hardly be done because of numerical limitations. In our calculations we have therefore used a constant spin and isospin independent "correlation energy" in order to shift the excited states down in energy with respect to the ground state bands of the nuclei considered. Obviously this is a rather crude approximation to the renormalization effects discussed above. However, it is the best we can do with the present computer facilities.

Note that this problem also appears in the RPA approach usually applied to describe the structure of the GMR's in spherical nuclei. There it is usually circumvented by renormalizing the ph force; i.e., one uses different forces to obtain the HF single particle energies and the ph spectrum. Such a prescription cannot be applied here, since in the open shell nuclei the spin projection operator mixes particle and hole states and therefore makes a clearcut separation of average field and residual interaction impossible.

With the energies and wave functions being so obtained, now the electromagnetic transitions between the various states can be calculated. For this purpose we shall first introduce the "spectroscopic amplitudes"

$$S_{fi}^{ab L^\pi}(\tau) = \langle f \| [C_{a_\tau}^+ C_{b_\tau}]^{L^\pi} \| i \rangle \tag{19}$$

for an arbitrary initial state $|i\rangle$ and final state $|f\rangle$ out of the set of wave functions (18). Here the reduced matrix element is defined according to Edmonds,[45] and the coupling convention

$$[C_{a_\tau}^+ C_{b_\tau}]_\mu^{L^\pi} = \delta(\pi_a \cdot \pi_b, \pi) \sum_{m_a m_b} (-)^{j_b - m_b} (j_a j_b L \,|\, m_a - m_b \mu) C_{a_\tau}^+ C_{b_\tau} \tag{20}$$

is used. Denoting by

$$Q^{L^\pi}(ab\tau) = \tfrac{1}{2}\{[1+\pi(-)^L]\langle a_\tau \| \hat{Q}(EL) \| b_\tau \rangle + [1-\pi(-)^L]\langle a_\tau \| \hat{Q}(ML) \| b_\tau \rangle\} \tag{21}$$

the reduced matrix elements of the L^π part of the usual long wavelength limit multipole expansion of the electromagnetic transition operator within our spherical single particle basis, we can then introduce a transition amplitude

$$T^{L^\pi}(fi) = \sum_{ab\tau} T_{ab\tau}^{L^\pi}(fi) = \sum_{ab\tau} \frac{1}{(2L+1)^{1/2}} Q^{L^\pi}(ab\tau) S_{fi}^{ab L^\pi}(\tau) \tag{22}$$

in terms of which the $B(EL)$—or $B(ML)$—values for the transitions between the states $|i\rangle$ and $|f\rangle$ can be expressed as

$$B(L^\pi; i \to f) = \frac{1}{2I_i + 1} |T^{L^\pi}(fi)|^2 . \tag{23}$$

The spectroscopic amplitudes could then directly be used to calculate the so called transition densities needed, for example, for a distorted-wave Born approximation (DWBA) analysis of inelastic electron or hadron scattering experiments. However, this has not been done in the present investigation.

III. THE CALCULATIONS

In the present work the model described above has been applied to ^{20}Ne and ^{28}Si. For both these nuclei all the $0s$, $0p$, $1s0d$, $1p0f$, and $0g_{9/2}$ orbits have been included in the model space basis, which therefore consisted of 100 spherical single nucleon states. As an effective nucleon-nucleon interaction the Brueckner G matrix of Barett, Hewitt, and McCarthy,[35] being based on the Hamada-Johnston potential,[49] has been used. Since the matrix elements of this interaction were available to the author only in an oscillator representation ($\hbar\omega = 14$ MeV), the one body terms of the total Hamiltonian (1), for which the matrix elements of the kinetic energy operator were taken, have also been calculated using oscillator wave functions of the same oscillator parameter.

It is well known that the matrix elements of a Brueckner G matrix depend on the so called "starting energy" ω, which appears in the energy denominator of the basic integral equation of Brueckner theory. Since this ω contains the Hartree-Fock single particle energies, in principle it should be determined self-consistently by a sort of Brueckner-Hartree-Fock procedure.[50] This has not been done in the present investigation. Instead, the starting energy ω has been fixed by the following, less sophisticated, prescription.

First, using the above Hamiltonian and single particle basis, Hartree-Fock calculations for the two spherical nuclei ^{16}O and ^{40}Ca have been performed. In these calculations for all those matrix elements involving more than one particle state (i.e., a state above the Hartree-Fock Fermi energy) the G matrix elements corresponding to a constant starting energy of $\omega = 40$ MeV have been taken. Otherwise ω has been interpolated. In the case of only hole states, i.e., for matrix elements of the type $v(\mathrm{h_1 h_2 h_3 h_4})$, $\omega = 2c + (\epsilon_{\mathrm{h_1}} + \epsilon_{\mathrm{h_2}} + \epsilon_{\mathrm{h_3}} + \epsilon_{\mathrm{h_4}})/2$ was used, while for matrix elements with but one particle state, i.e., of the types $v(\mathrm{h_1 h_2 h_3 p_1})$ or $v(\mathrm{h_3 p_1 h_1 h_2})$, $\omega = 2c + \epsilon_{\mathrm{h_1}} + \epsilon_{\mathrm{h_2}}$ was always assumed. The parameter c is a constant shift of the intermediate particle spectrum which has been introduced by Barett *et al.* in Ref. 35 and has been chosen here as 25 MeV for both spherical nuclei considered. The hole energies ϵ_{h} now have been

chosen such that the resulting Hartree-Fock single particle energy spectra roughly reproduce the experimental single neutron levels in ^{15}O and ^{39}Ca, respectively. Where these are not available, as, for example, in the case of the $1p0f$ orbits in ^{15}O, the theoretical values of Ref. 26 have been taken as the "experimental" standard. Values of $\epsilon_{0s} = -40$ MeV, $\epsilon_{0p} = -20$ MeV in ^{16}O and $\epsilon_{0s} = -60$ MeV, $\epsilon_{0p} = -42$ MeV, $\epsilon_{1s0d} = -20$ MeV in ^{40}Ca turned out to be suitable choices for this purpose. However, additionally the diagonal elements of the kinetic energy operator had to be modified for those orbits with a high orbital angular momentum 1. So the $0d$ orbits had to be shifted down by 1.8 MeV, the $0f$ levels by 5 MeV, and the $0g_{9/2}$ state by 4 MeV in ^{16}O in order to obtain reasonable agreement with the above defined standard. In ^{40}Ca the corresponding shifts were 2.5 MeV, 2.5 MeV, and 7 MeV, respectively. Though not proportional to $l(l+1)$, these shifts could be interpreted as a sort of l^2 term which somehow corrects for the unrealistic shape of the basis creating oscillator potential. Note that our above choice of the hole energies does not include such l^2 effects. Neither does it take into account the one body spin orbit force. Probably, at least part of the additional shifts introduced here could be avoided by allowing for a more complicated hole energy spectrum than the one which has been chosen here for the sake of simplicity.

Using the two so defined Hamiltonians for ^{16}O and ^{40}Ca, the Hartree-Fock single particle energy spectra at the extreme left and extreme right, respectively, of Fig. 1 are obtained. Except for the $0s_{1/2}$ orbits, which come out too tightly bound in both cases, a reasonable agreement with the above standard is reached. Note, that the "0" here always indicates the lowest orbit for a given total and orbital angular momentum. Actually, since we allow major shell mixing, for example, the $0s_{1/2}$ states in Fig. 1 are mixtures of the $0s_{1/2}$ and $1s_{1/2}$ oscillator orbits.

For the two open shell nuclei ^{20}Ne and ^{28}Si the corresponding Hamiltonians have now been obtained by a linear interpolation of all the two body matrix elements as well as of the shifts for the high l diagonal one body terms between the values derived for ^{16}O and ^{40}Ca in the above described way. With these Hamiltonians intrinsic Hartree-Fock calculations for both nuclei have then been performed. As already mentioned in the last section, in these calculations axial symmetry was imposed on the Hartree-Fock orbits and the Coulomb force was neglected. Both these approximations can be easily justified for ^{20}Ne as well as for ^{28}Si. It is known from earlier calculations[40] that the lowest intrinsic Hartree-Fock solutions in both

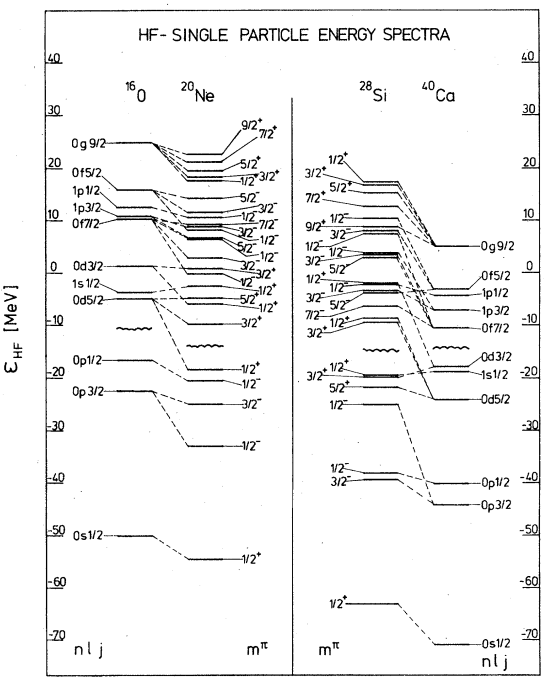

FIG. 1. The Hartree-Fock single particle energies ϵ_{HF} (MeV) for ^{16}O, ^{20}Ne, ^{28}Si, and ^{40}Ca as obtained with the BHM G matrix (Ref. 35) in the version discussed in Sec. III. The orbits of the two spherical nuclei are labeled with the oscillator quantum numbers nlj (because of the neglect of the Coulomb force proton and neutron orbits are degenerate). The fourfold degenerate orbits (spin up and down for both proton and neutron) of the two axially deformed Hartree-Fock solutions for ^{20}Ne (prolate) and ^{28}Si (oblate) are characterized by their spin projection and parity m^π. The connections (dashed lines) between the spherical and deformed levels indicate the maximum component of the latter. The wiggly lines give the Fermi surfaces in the nuclei considered.

these nuclei are axially deformed, yielding a prolate shape for ^{20}Ne and an oblate configuration for ^{28}Si. In both cases the Hartree-Fock solutions with other deformations turn out to be considerably higher in energy, at least if a reasonable effective interaction is used within the chosen model space. So, for example, taking the Kuo force[51] and an $1s0d$-shell basis, the prolate solution for ^{28}Si is about 4 MeV less bound than the oblate one.[52] Furthermore, in these light doubly even $N=Z$ nuclei the Coulomb force essentially only shifts the proton single particle energies relative to those of the neutrons but leaves the corresponding single particle wave functions almost unchanged. Its neglect here can therefore also be considered a reasonable approximation.

As in the older calculations, we also obtain a prolate solution for ^{20}Ne and an oblate shape for

^{28}Si. The corresponding self-consistent single particle spectra are again displayed in Fig. 1 (mid-left and mid-right sides for ^{20}Ne and ^{28}Si, respectively). Each orbit is labeled by its total angular momentum projection m on the intrinsic symmetry axis and its parity π. Because of the above mentioned approximations each level is fourfold degenerate and can be occupied by a proton, a neutron, and their time reversed partners. The dashed lines to the Hartree-Fock spectra of ^{16}O and ^{40}Ca indicate the main spherical component of the various deformed states.

As can be easily seen, the Hartree-Fock procedure produces large energy gaps between the occupied and unoccupied orbits in both nuclei. This is an indication of the relative stability of the corresponding intrinsic ground states even against 2p2h and higher order correlations and agrees also with the results of older calculations. Indeed, neither the inclusion of $T=0$ pairing via the Hartree-Fock Bogoliubov theory[53] nor of even more complicated correlations as done, for example, in the Multi-Configuration-Hartree-Fock approach[52] yields considerable contributions to the intrinsic Hartree-Fock ground states of ^{20}Ne and ^{28}Si. At least for the ground state band of these nuclei, the PHM method, which in addition even includes some spin dependent renormalization effects on the Hartree-Fock field via the admixture of angular momentum projected 1p1h configurations, should therefore be considered a rather good approximation.

The so obtained self-consistent deformed orbits have now been used to construct the overlap, energy, and center of mass energy matrices within the nonorthogonal angular momentum projected configurations (16) and (17). For each considered parity, spin, and isospin value all the configurations of these two types which could be constructed in the chosen model space, were always taken into account. The dimensions of the resulting configuration spaces are listed in Table I. Almost all the configurations counted there are of the four-determinantal 1p1h structure (17). Only for the isoscalar positive parity states with even spins does the angular momentum projected reference determinant (16) contribute to the total wave functions.

As already discussed in Sec. II, the spurious admixtures due to the center of mass motion had to be removed before proceeding. For this purpose the center of mass Hamiltonian was diagonalized in all the different configuration spaces corresponding to the various spin, isospin, and parity quantum numbers which have been considered in the present study. As expected, in all cases those states corresponding to a center of mass excitation turned out to be energetically well separated from those states at energies near the zero point energy of the center of mass motion and could hence easily be removed from the matrix equation (10) for the many nucleon Hamiltonian (1). Obviously, as already mentioned, this elimination is not exact: Our configuration spaces are far from being complete with respect to the center of mass Hamiltonian and furthermore, due to the inclusion of major shell mixing, the reference determinant (4) already contains some spurious center of mass admixtures. However, after removing, for example, the spurious isoscalar 1^- states in the approximate way described above, the total energy weighted isoscalar electric dipole strength, which is some measure for the remaining spuriousity, turned out to be less than about 5% of the corresponding isovector transition strengths in both nuclei. We think that this is an amount of residual spurious admixtures, which should not influence the results too drastically.

TABLE I. The dimensions of the configuration spaces used for the different spin, parity, and isospin values in ^{20}Ne and ^{28}Si are displayed. Most of the configurations are of the particle-hole structure (17). Only for the isoscalar positive parity states with even spins does the angular momentum projected reference determinant (16) contribute to the total wave functions.

Nucleus	^{20}Ne		^{28}Si	
Isospin	$T=0$	$T=1$	$T=0$	$T=1$
$I^\pi=0^+$	18	17	21	20
0^-	17	17	21	21
1^+	49	49	57	57
1^-	48	48	59	59
2^+	75	74	87	86
2^-	72	72	88	88
3^+	89	89	105	105
3^-	88	88	108	108
4^+	98	97	117	116
4^-	96	96	120	120
5^+	100	100	121	121
5^-	99	99	126	126
6^+	101	100	124	123
6^-	100	100	128	128

With the spurious center of mass admixtures being eliminated at least approximately, the energies and wave functions for the two nuclei considered were calculated via solving the matrix equation (10) in the various configuration spaces.

As already discussed in Sec. II, there is some inconsistency inherent in the PHM description of the excited states with respect to that of the ground state band due to the truncation of the configuration spaces after the angular momentum projected 1p1h configurations. It has been argued

that in order to take into account the strong renormalization effects due to collective $2\hbar\omega$ excitations, which have been discussed in detail in Ref. 48, in principle at least part of the spin projected 2p2h configurations should be included in the configuration spaces, not only for the ground state bands but also for the excited states. However, since this extension would complicate the numerical calculations enormously, we decided to simulate the influence of these collective excitations on the excited states by a spin and isospin independent constant correlation energy $\Delta E_c(\pi)$, which shifts the excited states of parity π down in energy with respect to the ground state band. Obviously this is a rather rough approximation; however, since it is the best we can do with the present computer facilities, we have no other choice. The correlation energies $\Delta E_c(+)$ were then fixed by renormalizing the lowest isoscalar 3^+ states in both nuclei to the experimental excitation energies. For this purpose, in ^{20}Ne a value of $\Delta E_c(+) = 2.7$ MeV was needed, and in ^{28}Si a value of $\Delta E_c(+) = 2.2$ MeV was needed. In ^{28}Si the same shift of 2.2 MeV was also applied to the negative parity spectrum. In ^{20}Ne, however, a value of $\Delta E_c(-) = 4.25$ MeV had to be used in order to get the negative parity states sufficiently down in energy. Here the lowest isoscalar 3^- state was used for the additional renormalization. Note that—with the Hamiltonian (1) assumed as given—these three correlation energies are the only free parameters in the present calculations.

Then the spectroscopic amplitudes (19) in both nuclei were calculated. Though being able to calculate these amplitudes between two arbitrary states of the type (18), in the present investigations our computer code was only used to evaluate those transitions involving the ground state as the initial state. These spectroscopic amplitudes represent a decomposition of the various excitations of the system into spherical particle-hole components and therefore yield some valuable information about the structure of the wave functions.

The electromagnetic transitions from the ground to the various excited states were then calculated according to Eqs. (22) and (23). For this purpose the reduced single particle matrix elements of the various multipole components of the electromagnetic transition operator are needed, which, to be consistent, in principle should be calculated within the same single particle basis functions as were used for the many body Hamiltonian. However, one may also adopt the point of view that the Hamiltonian (1) is an effective matrix depending only on the quantum numbers of the various states involved. This is, for example, done in some large shell model calculations treating all the one and two body terms of (1) as free parameters to be determined by a least square fit of the theoretical results to the experimental data.[54] At least to some extent it is therefore justified to investigate the influence of different single particle basis functions for the electromagnetic transition operator and to leave the Hamiltonian (1), and hence the energies and spectroscopic amplitudes of the system, unchanged. Therefore in the present paper besides the harmonic oscillator representation for the transition operator a more realistic Woods-Saxon basis has also been studied.

For the construction of this basis the usual Woods-Saxon Hamiltonian

$$h_{\mathrm{WS}} = -\frac{\hbar^2}{2\mu}\Delta + V^{lj}(r) \tag{24}$$

was taken, where $\mu = m(A-1)/A$ (m being the average nucleon mass) is the reduced mass of the system and the potential $V^{lj}(r)$ is given by

$$V^{lj}(r) = U_0 f(r) + U_{ls}\left(\frac{\hbar^2}{m_\pi c}\right)^2 \times [\,j(j+1) - l(l+1) - \tfrac{3}{4}]\frac{1}{r}\frac{df(r)}{dr} \tag{25}$$

with m_π being the pion mass. The radial dependence $f(r)$ has the form

$$f(r) = \left[1 + \exp\left(\frac{r-R}{a}\right)\right]^{-1}, \tag{26}$$

where $R = r_0(A-1)^{1/3}$ is the nuclear radius and a the usual diffuseness parameter. The Coulomb force has here been neglected, since we consider only doubly even $N=Z$ nuclei and assume degenerate orbits for protons and neutrons. The parameters for this potential ($U_0 = -53.14$ MeV, $U_{ls} = -5.186$ MeV, $r_0 = 1.25$ fm, and $a = 0.53$ fm) have been taken without any change from Ref. 26 and have been used for ^{20}Ne as well as for ^{28}Si.

For each considered orbital and total angular momentum (l and j, respectively), the Hamiltonian (24) was diagonalized in an oscillator basis including all oscillator wave functions $R_{nl}(r)$ with node numbers $n=0$ to $n=9$. This procedure yields very accurate results for the bound solutions of (24), but, however, fails for the continuum states of this Hamiltonian. In order to discretize the latter we therefore adopted a procedure which was first proposed by Speth and collaborators[34] and has also been used in Refs. 26 and 28. In this method, the continuum solutions of (24) are first expanded in the same oscillator basis as used for the bound states with the same spin quantum numbers. The expansion coefficients $a_{nlj}(E)$, which now depend on energy, are then averaged over some energy interval Δ around the energy E_R

TABLE II. The Woods-Saxon single nucleon wave functions used for the electromagnetic transition operators in ^{20}Ne are given in terms of their expansion coefficients in an harmonic oscillator basis. For the unbound orbits the energy intervals Δ, over which the wave functions have been averaged, are given in addition. States marked by an asterisk do not show a single particle resonance. They have been energy averaged around the first maximum of $\sin^2\delta$, where δ is the scattering phase.

n \ αlj	$Os_{\frac{1}{2}}$	$Op_{\frac{3}{2}}$	$Op_{\frac{1}{2}}$	$Od_{\frac{5}{2}}$	$1s_{\frac{1}{2}}$	$Od_{\frac{3}{2}}$	$Of_{\frac{7}{2}}$	$1p_{\frac{3}{2}}^*$	$1p_{\frac{1}{2}}^*$	$Of_{\frac{5}{2}}$	$Og_{\frac{9}{2}}$
Δ(MeV)							1.36	7.12	5.16	7.66	10.8
0	0.999	0.999	0.999	0.994	0.035	0.978	0.921	0.026	0.028	0.863	0.848
1	−0.037	−0.017	−0.003	−0.052	0.956	−0.104	−0.214	0.829	0.718	−0.092	0.056
2	−0.016	0.013	0.031	0.078	−0.189	0.145	0.232	−0.341	−0.437	−0.016	−0.161
3	−0.020	−0.032	−0.031	−0.058	0.165	−0.088	−0.157	0.237	0.390	0.197	0.294
4	−0.002	−0.003	−0.002	0.014	−0.122	0.047	0.081	−0.100	−0.285	−0.267	−0.280
5	0.001	−0.004	−0.007	−0.019	0.061	−0.042	−0.043	−0.036	0.166	0.260	0.169
6	0.002	0.002	0.002	0.009	−0.050	0.024	−0.009	0.111	−0.074	−0.217	−0.051
7	0.001	0.001	−0.000	−0.005	0.030	−0.017	0.047	−0.173	−0.015	0.138	−0.066
8	0.001	0.001	0.001	0.004	−0.017	0.011	−0.079	0.203	0.083	−0.054	0.142
9	0.000	0.000	0.000	−0.001	0.010	−0.004	0.106	−0.212	−0.137	−0.025	−0.174

$$\tilde{a}_{nlj}(E_R) = \int_{E_R-\Delta/2}^{E_R+\Delta/2} a_{nlj}(E)dE\,, \tag{27}$$

where E_R is either the resonance energy in the considered single particle channel or, if no single particle resonance is obtained, given by the first maximum of $\sin^2\delta_{lj}(E)$, where $\delta_{lj}(E)$ is the scattering phase. Δ is usually chosen such that $\sin^2\delta_{lj}(E)$ adopts about half its maximum value at $E_R-\Delta/2$. The resulting energy averaged wave function (27) is then finally orthonormalized with respect to all the already obtained solutions (bound and unbound) with the same spin quantum numbers l and j.

The Woods-Saxon wave functions so obtained for ^{20}Ne and ^{28}Si are given in terms of their oscillator expansion coefficients in Tables II and III, respectively. It is easily seen that the bound orbits in both nuclei are almost pure oscillator states (maximum deviation 8.6% for the $1s_{1/2}$ orbit in ^{20}Ne). To some extent this is even true for the $0f_{7/2}$ resonance in ^{20}Ne, which because of the large centrifugal barrier is relatively narrow and still has an overlap of about 85% with the corresponding oscillator wave function. For the higher states, however, oscillator and Woods-Saxon wave functions are rather different. So, for example, the $1p_{1/2}$ state in ^{20}Ne has only a 51% overlap with the $1p_{1/2}$ oscillator orbit and shows large admixtures from the higher oscillator shells.

It should be pointed out here that the inclusion of even higher shells ($n>9$) in the oscillator expansion still has considerable effects on the tails of the radial wave functions of the unbound states. Therefore if quantities which are sensitive to these tails have to be calculated, for example, the transition densities to be used for inelastic α scattering, these higher shells have to be taken into account. For the electromagnetic transitions with multipolarities $L\leq 4$, however (only these will be studied in the present investigation), an increase of the oscillator basis from $n\leq 9$ to

TABLE III. Same as in Table II, but for the nucleus ^{28}Si.

n \ αlj	$Os_{\frac{1}{2}}$	$Op_{\frac{3}{2}}$	$Op_{\frac{1}{2}}$	$Od_{\frac{5}{2}}$	$1s_{\frac{1}{2}}$	$Od_{\frac{3}{2}}$	$Of_{\frac{7}{2}}$	$1p_{\frac{3}{2}}$	$1p_{\frac{1}{2}}^*$	$Of_{\frac{5}{2}}$	$Og_{\frac{9}{2}}$
Δ(MeV)								0.03	2.58	0.70	2.38
0	0.998	0.999	0.999	0.999	0.054	0.997	0.987	0.011	−0.007	0.913	0.888
1	−0.056	−0.009	0.017	0.009	0.991	0.015	−0.050	0.754	0.852	−0.189	−0.173
2	−0.031	−0.014	−0.001	0.027	−0.068	0.006	0.117	−0.291	−0.324	0.259	0.185
3	−0.018	−0.030	−0.029	−0.042	0.073	−0.043	−0.086	0.292	0.302	−0.183	−0.057
4	0.000	−0.005	−0.006	−0.003	−0.069	0.003	0.033	−0.271	−0.223	0.127	−0.056
5	0.003	−0.001	−0.003	−0.008	0.013	−0.014	−0.038	0.291	0.125	−0.098	0.114
6	0.003	0.003	0.002	0.004	−0.018	0.004	0.021	−0.211	−0.075	0.051	−0.170
7	0.001	0.002	0.001	0.001	0.011	−0.002	−0.014	0.191	0.014	−0.018	0.189
8	0.000	0.001	0.001	0.002	−0.003	0.003	0.010	−0.177	0.032	−0.014	−0.186
9	−0.000	0.000	0.000	0.000	0.005	0.000	−0.003	0.167	−0.070	0.044	0.166

$n \leq 14$ had only minor effects on the Woods-Saxon transition matrix elements and could hence safely be neglected.

Though being obviously more "realistic" than the oscillator basis, the use of the Woods-Saxon wave functions introduces some ambiguity. If, for example, the depth of the potential is increased, the wave functions of the bound orbits remain almost unchanged; the unbound solutions, however, become more similar to the corresponding oscillator orbits. A decrease of the depth has the opposite effect. One therefore should not overstress the results obtained with the Woods-Saxon basis but rather consider them mainly as some tool to study the qualitative changes induced by an improvement of the single particle wave functions.

With the single particle wave functions being so obtained, the electromagnetic transitions from the ground to the various excited states were calculated. Neither effective charges nor effective g factors were introduced. For electric transitions a proton charge of $1|e|$ and a neutron charge of 0 were always used, and for magnetic transitions the free g factors ($g_l(p)=1$, $g_l(n)=0$, $g_s(p)=5.5857$, $g_s(n)=-3.8263$, all in nuclear magnetons [μ_K]) were always assumed. From the $B(EL)$ or $B(ML)$ values for the various transitions the theoretical energy weighted sumrules

$$\Sigma^T_{\text{calc}}(L^\pi) = \sum_{f(L^\pi)} \Delta E_f \, B(L^\pi; \text{g.s.} \rightarrow f) \tag{28}$$

were then obtained. Here g.s. denotes the ground state, T may adopt the value 0 (isoscalar) or 1 (isovector transitions), and the sum runs over all final states f with spin and parity L^π and excitation energy ΔE_f.

These theoretical sumrules can then be compared to the well known classical predictions for the energy weighted transition strengths, which for $N=Z$ nuclei and $r_0=1.2$ fm can be written as[55]

$$\Sigma^{T=0}_{\text{cl}}(E0) = \Sigma^{T=1}_{\text{cl}}(E0) = 56.91 Z^{5/3} \quad (e^2\text{fm}^4\text{MeV}) \tag{29}$$

for electric monopole transitions,

$$\Sigma^{T=0}_{\text{cl}}(EL) = \Sigma^{T=1}_{\text{cl}}(EL) = 2.48 \cdot (2)^{(2L-2)/3} \cdot (1.2)^{2L-2} \cdot L(2L+1) \cdot Z^{(2L+1)/3} \quad (e^2\,\text{fm}^{2L}\,\text{MeV}) \tag{30}$$

for electric transitions with $L \geq 2$, and finally as

$$\Sigma^{T=1}_{\text{cl}}(E1) = 7.43 \cdot Z \cdot (1+\chi) \quad (e^2\text{fm}^2\text{MeV}) \tag{31}$$

for the famous electric dipole transitions.

The dimensionless parameter χ in (31) describes the influence of velocity dependent terms in the residual interaction and has been chosen here as 0.5.[56] Obviously, similar correction terms are also expected for the other classical sumrules. However, since nothing is known about their magnitude (except that they should be larger for the isovector transitions, where protons and neutrons move in opposite directions and hence with a large relative velocity than for the isoscalar transitions, where protons and neutrons move in phase[55]), in the present study no such corrections have been implied.

IV. RESULTS AND DISCUSSION

The low energy spectra of ^{20}Ne and ^{28}Si are presented in Fig. 2. The results of our angular momentum projected deformed particle-hole approach (PHM) are compared with the experimental data[57] (EXP) and, as far as the ground state bands are considered, also with the levels obtained by projecting angular momentum only from the intrinsic reference determinant (16) (HF). Each state is labeled by its total angular momentum I. Uncertain experimental spin assignments are indicated by parentheses. The theoretical states with different isospins are distinguished by giving the corresponding spin labels in different columns, and experimental isospin assignments different from zero are indicated by a second label in parentheses. As discussed in the last section, in both nuclei the lowest 3^+ states have been used to determine the "correlation energy" introduced in Sec. II. In ^{20}Ne the lowest isoscalar 3^- state has additionally been used for this purpose.

Comparing the HF spectra with the PHM ground state bands it is seen that the inclusion of the angular momentum projected 1p1h configuration (17) here yields far less pronounced energy gains than reported in Ref. 48. This is due to the fact that most of the strongly collective $2\hbar\omega$ excitations, which had been studied explicitly in Ref. 48, here were already taken into account in the mean field via the inclusion of major shell mixing in the self-consistent HF orbits (2). Nevertheless, the energy gains due to the projected 1p1h admixtures are still considerable and increase with increasing spin, indicating a non-negligible angular momentum dependence of the correlations in the ground state bands. As already discussed in Sec. II, such spin dependent renormalization effects are also obtained if the projection is performed before the variation of the HF field. In fact, test calculations[58] with the modified surface delta interaction[37] in an $1s0d$ shell basis showed that, for the 0^+ ground states of ^{20}Ne and ^{28}Si, the PHM approach and the HF model with spin projection

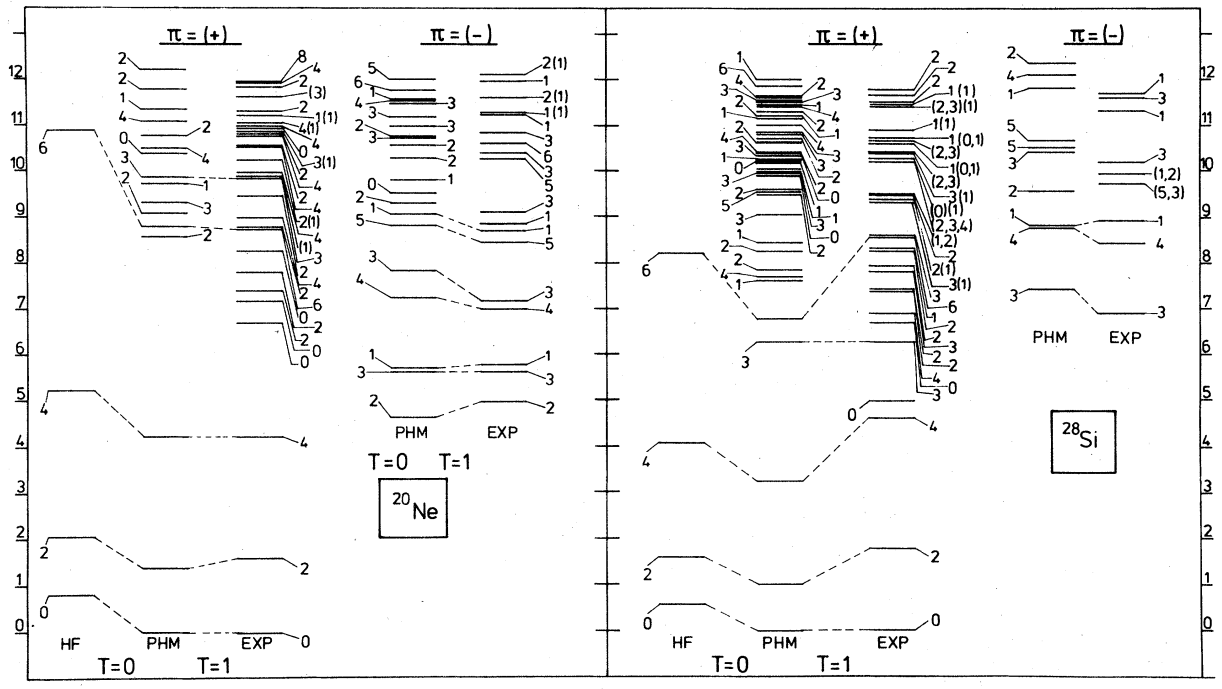

FIG. 2. The low energy spectra of ^{20}Ne and ^{28}Si as obtained by angular momentum projection from the intrinsic Hartree-Fock solutions (HF) are compared with the results of our multideterminant approach (PHM) as well as with the experimental data (EXP) (Ref. 57). All the states are labeled by their total angular momenta. In a case where two indices are given for an experimental level the second one (in parentheses) indicates the total isospin. In both nuclei the lowest isoscalar 3^+ state has been used in order to determine the correlation energy discussed in Sec. II. In ^{20}Ne in addition the lowest 3^- state has been used for this purpose.

before the variation of an axially deformed field yield almost identical results. For the 2^+-members of the ground state bands, however, the PHM solutions are already energetically favored since they include nonaxial contributions (essentially from the $K = 2$ 1p1h configurations) which are not taken into account by the axially symmetric HF wave functions.

For the ground state band of ^{20}Ne the agreement of the theoretical and the experimental excitation energies is rather good. This result is quite satisfying, since it was obtained using a microscopic G matrix in a large model space and not by a SCM diagonalization with a fitted effective interaction inside only one major shell. It may hence be considered some indication that the essential physical structures of the ground state band in ^{20}Ne are already contained in the relatively simple wave functions (18) used in the present investigation. For ^{28}Si this statement holds only to some extent. Here the theoretical spectrum is too compressed. Nevertheless, for a completely microscopic calculation like the present one, the agreement with the experimental data may even here be considered encouraging.

Good agreement with the experimental data is also obtained for the excitation energies of the low excited negative parity states in both nuclei. Level ordering as well as relative spacing are well reproduced by the calculations. This result supports a particle-hole structure of the type (18) for these states also and shows furthermore that our crude assumption of a spin and isospin independent correlation energy seems to be a reasonable approximation, at least for the negative parity states.

For the low excited positive parity levels in both nuclei the agreement is much worse. So, for example, in ^{20}Ne none of the experimental positive parity states between 6 and 8 MeV excitation energy are reproduced, and also in ^{28}Si many states in this energy region are missing. However, this defect of the PHM approach can be easily understood; It is well known from older calculations[59] that most of the low excited 0^+ states in ^{20}Ne (and the rotational bands being based on them) very likely have to be interpreted as 4p4h "quartet" structures relative to the intrinsic HF ground state. Since now, as has already been discussed in Sec. II, the PHM wave functions (18) take into account at most 3p3h excitations with respect to the latter, these states are not included

in our configuration space and hence cannot be reproduced. Similar arguments hold for ^{28}Si, where in addition to the quartet excitations, the lowest 0^+ state (and the rotational states being based on it) can be easily identified as a prolate configuration which cannot be described by only few particle-few hole excitations with respect to the oblate ground state. Note that the (RPA) (Refs. 25 and 26) and even the core-coupling-random phase (CRPA) (Refs. 27 and 18) approaches, which have been successfully used recently for the description of the structure of the GMR's in closed shell nuclei, suffer from the same defect. They also fail to reproduce the low excited many particle-many hole states; for example, the first excited 0^+ in ^{16}O, which is most probably of 4p4h structure.

Obviously, a comparison of only the excitation energies with the experimental data is not sufficient to judge the quality of the PHM approach for the ground state bands and the low excited states of the two nuclei considered. Other properties of the wave functions, for example, occupation numbers and electromagnetic transition probabilities, should be investigated. This is done in Tables IV–VII.

Table IV shows the occupation numbers for the spherical single particle states in the PHM ground states of ^{20}Ne and ^{28}Si and, more for completeness than for comparison, also shows the predictions of the naive independent particle model (IPM) for these quantities. As far as the $1s0d$ levels are considered, these occupation numbers can be compared with the experimental data deduced from the analysis of direct transfer reactions and with the results of other calculations reported in Ref. 60. For ^{20}Ne, experiment[61] obtains 1.8 nucleons in the $0d\frac{5}{2}$ orbit, 1.85 in the $1s\frac{1}{2}$ level, and 0.35 in the $0d\frac{3}{2}$ state, while the PHM approach predicts 2.09, 1.39, and 0.62 nucleons in these three orbits, respectively. Castel *et al.*[60] using the Kuo force[51] and an $1s0d$ basis in Hartree-Fock calculations with (approximate) angular momentum projection before the variation, obtained occupation numbers of 2.0 ($0d\frac{5}{2}$), 1.68 ($1s\frac{1}{2}$), and 0.32 ($0d\frac{3}{2}$) nucleons. In ^{28}Si, experiment[62] suggests 8.52, 1.59, and 1.89 nucleons in the three $1s0d$ orbits, while our calculations yield 6.88, 2.57, and 2.54 particles. Castel *et al.*[60] report values of 8.78, 1.40, and 1.82 nucleons, respectively. Other recent calculations[21,54] here predict a $0d\frac{5}{2}$ occupation between 6.84 and 9.1 nucleons, depending on the choice of the effective interaction. Taking into account the uncertainties in the deduction of the experimental occupation numbers as well as the strong dependence of the results obtained using only the $1s0d$ shell basis on the choice of the residual interaction, one has to conclude that the PHM approach reproduces the experimental data as well as the results of the other calculations. Note that all occupation numbers used here for comparison with our results have been deduced by assuming an inert ^{16}O core and a total $1s0d$ occupation of 4 or 12 nucleons for ^{20}Ne or ^{28}Si, respectively. As can be seen from our results, the second assumption seems to be rather well fulfilled, even if core excitations are taken into account. However, the PHM occupation numbers also show that there is a non-negligible probability to find a hole in the ^{16}O core and a particle outside the $1s0d$ shell in the ^{20}Ne as well as in the ^{28}Si ground state.

TABLE IV. The ground state occupation numbers for the the various spherical orbits in ^{20}Ne and ^{28}Si as obtained from our particle-hole model (PHM) are compared with the predictions of the simple independent particle model (IPM)

Nucleus	^{20}Ne		^{28}Si	
nlj \ Model	IPM	PHM	IPM	PHM
$Os\frac{1}{2}$	4	3.86	4	3.90
$Op\frac{3}{2}$	8	7.64	8	7.73
$Op\frac{1}{2}$	4	3.82	4	3.86
$Od\frac{5}{2}$	4	2.09	12	6.88
$1s\frac{1}{2}$	0	1.39	0	2.57
$Od\frac{3}{2}$	0	0.62	0	2.54
$Of\frac{7}{2}$	0	0.14	0	0.16
$1p\frac{3}{2}$	0	0.19	0	0.06
$1p\frac{1}{2}$	0	0.05	0	0.02
$Of\frac{5}{2}$	0	0.16	0	0.17
$Og\frac{9}{2}$	0	0.04	0	0.11
Os shell	4	3.86	4	3.90
Op shell	12	11.46	12	11.59
$1s0d$ shell	4	4.10	12	11.99
$1p0f$ shell	0	0.54	0	0.41
$Og\frac{9}{2}$ shell	0	0.04	0	0.11
Total	20	20.00	28	28.00

Table V displays the proton spectroscopic amplitudes (19) for $L^\pi = 2^+$ transitions between the ground and the first excited $I^\pi = 2^+$ states in the two considered nuclei and compares them with the results of complete $1s0d$ shell SCM calculations using a fitted effective Hamiltonian, which have been recently reported by Chung and Wildenthal.[63] Obviously, due to the inclusion of a much larger model space, the PHM model here yields much

TABLE V. The spectroscopic amplitudes (19) for proton isoscalar electric quadrupole transitions from the ground to the lowest $I^\pi = 2^+$ states in both nuclei are displayed and compared with the values obtained by an sd-shell shell model configuration mixing (SCM) calculation by Chung and Wildenthal (Ref. 63).

	Nucleus	^{20}Ne		^{28}Si	
	Method	PHM	SCM	PHM	SCM
	State no.	1	1	1	1
a	b \ ΔE (MeV)	1.38	1.75	1.01	2.19
$Os\frac{1}{2}$	$Od\frac{3}{2}$	0.1025		−0.1168	
	$Od\frac{5}{2}$	0.1083		−0.1354	
$Op\frac{1}{2}$	$Op\frac{3}{2}$	−0.0155		−0.0081	
	$1p\frac{3}{2}$	−0.0778		0.0543	
	$Of\frac{5}{2}$	0.2323		−0.2418	
$Op\frac{3}{2}$	$Op\frac{1}{2}$	0.0147		0.0086	
	$Op\frac{3}{2}$	−0.0014		0.0089	
	$1p\frac{1}{2}$	0.0797		−0.0671	
	$1p\frac{3}{2}$	0.0781		−0.0629	
	$Of\frac{5}{2}$	0.1216		−0.1383	
	$Of\frac{7}{2}$	0.2454		−0.2810	
$1s\frac{1}{2}$	$Od\frac{3}{2}$	−0.2628	−0.2593	0.2070	0.1439
	$Od\frac{5}{2}$	−0.5636	−0.5629	0.6366	0.9250
$Od\frac{3}{2}$	$Os\frac{1}{2}$	−0.1025		0.1223	
	$1s\frac{1}{2}$	0.4104	0.3447	−0.3697	−0.2482
	$Od\frac{3}{2}$	−0.1746	−0.1803	0.5669	0.3099
	$Od\frac{5}{2}$	0.1753	0.1692	−0.6433	−0.5913
$Od\frac{5}{2}$	$Os\frac{1}{2}$	0.1043		−0.1346	
	$1s\frac{1}{2}$	−0.7484	−0.6467	0.7341	0.6388
	$Od\frac{3}{2}$	−0.1485	−0.1518	0.6120	0.4870
	$Od\frac{5}{2}$	−0.5309	−0.6435	0.7788	0.4949
	$Og\frac{9}{2}$	0.0593		−0.1395	
$1p\frac{1}{2}$	$Op\frac{3}{2}$	−0.0885		0.0739	
	$1p\frac{3}{2}$	−0.0168		0.0107	
	$Of\frac{5}{2}$	0.0176		−0.0143	
$1p\frac{3}{2}$	$Op\frac{1}{2}$	0.0763		−0.0538	
	$Op\frac{3}{2}$	0.0801		−0.0651	
	$1p\frac{1}{2}$	0.0162		−0.0104	
	$1p\frac{3}{2}$	0.0203		−0.0114	
	$Of\frac{5}{2}$	0.0149		−0.0107	
	$Of\frac{7}{2}$	0.0282		−0.0217	
$Of\frac{5}{2}$	$Op\frac{1}{2}$	0.2528		−0.2573	
	$Op\frac{3}{2}$	−0.1281		0.1439	
	$1p\frac{1}{2}$	0.0181		−0.0144	
	$1p\frac{3}{2}$	−0.0143		0.0104	

TABLE V. (*Continued*).

	Nucleus		^{20}Ne		^{28}Si	
	Method		PHM	SCM	PHM	SCM
	State no.		1	1	1	1
	ΔE (MeV)		1.38	1.75	1.01	2.19
a	b					
	$Of_{\frac{5}{2}}$		−0.0325		−0.0301	
	$Of_{\frac{7}{2}}$		0.0126		0.0108	
$Of_{\frac{7}{2}}$	$Op_{\frac{3}{2}}$	0.2642		−0.2978		
	$1p_{\frac{3}{2}}$	0.0310		−0.0238		
	$Of_{\frac{5}{2}}$	−0.0125		−0.0113		
	$Of_{\frac{7}{2}}$	−0.0249		−0.0274		
$Og_{\frac{9}{2}}$	$Od_{\frac{5}{2}}$	0.1034		−0.1908		
	$Og_{\frac{9}{2}}$	−0.0088		−0.0124		

more information than the latter approach, which is restricted to only the $1s0d$ shell. However, comparing just the $1s0d$ shell spectroscopic amplitudes, one observes that in ^{20}Ne the values predicted by the two different approaches agree surprisingly well, and even in ^{28}Si, where, as already mentioned, the PHM description of the ground state band is not as satisfying as in ^{20}Ne, the SCM amplitudes are still qualitatively well reproduced. The quantitative discrepancies are very likely due to the different $0d_{\frac{5}{2}}$ occupation obtained by the two approaches (6.88 nucleons in the PHM, 9.10 particles[21] in the SCM calculations), which is not necessarily attributable to the PHM truncation of the configuration space but could also be caused by the differences of the two Hamiltonians.

Calculating the 0^+-2^+ $B(E2)$ values for the two nuclei with the spectrocopic amplitudes from Table V, it turns out that the SCM approach, being restricted to excitations only inside the $1s0d$ shell, has to introduce an effective extra charge of about $0.5e$ for both protons and neutrons in order to reproduce the experimental $B(E2)$ values of 287 ± 40 e^2fm^4 in ^{20}Ne (Ref. 64) and 326 ± 10 e^2fm^4 in ^{28}Si.[65] Owing to the inclusion of core excitations, the PHM calculations here already obtain 195 e^2fm^4 and 315 e^2fm^4 using the bare $E2$ transition operator (in the Woods-Saxon representation; for harmonic oscillator wave function values of 165 e^2fm^4 and 347 e^2fm^4 are obtained), and hence only a very small extra charge in ^{20}Ne ($\sim 0.1e$) and no effective charge at all in ^{28}Si is needed.

Similar remarks apply to the $L^\pi = 4^+$ proton spectroscopic amplitudes (19) connecting the ground with the first and first two excited 4^+ states in ^{20}Ne and ^{28}Si, respectively, which are presented in Table VI. For the 4^+ state in ^{20}Ne rather good agreement with the SCM data of Chung and Wildenthal[63] is obtained. The large quantitative discrepancies, especially in the $(0d_{\frac{5}{2}} - 0d_{\frac{5}{2}})$ amplitudes for the first two 4^+ states in ^{28}Si, once more indicate that here the SCM and the PHM approaches yield, as far as the $1s0d$ shell part is considered, somewhat different wave functions.

The large similarity between the PHM and SCM descriptions, at least for ^{20}Ne, is not only restricted to the ground state band but also persists for other excited states. This can be seen from Table VII, where the proton spectroscopic amplitudes (19) for the $I^\pi = 1^+$ state, which carries most of the magnetic dipole transition strength in ^{20}Ne and ^{28}Si, are presented. In both models this state turns out to be the first excited $1^+(T=1)$ state in ^{20}Ne and the third $1^+(T=1)$ level in ^{28}Si. As far as the excitation energies of these two states are considered, one has to admit that the SCM results[66] agree much better with experiment than the PHM values, which are about 1.5 and 2 MeV too low. However, since the PHM approach is based on a completely microscopic Hamiltonian with the kinetic energy operator as a one body term and only a crude assumption of a constant correlation energy for all the excited states, while the SCM approach uses effective single particle energies and two body terms both fitted to various experimental data, an ambiguity of about 1.5 MeV in this excitation energy region should not be taken too seriously. The PHM spectroscopic amplitudes for the $1s0d$ part of the first isovector 1^+ excitation in ^{20}Ne are again nearly

TABLE VI. The spectroscopic amplitudes (19) for proton isoscalar electric hexadecapole transitions from the ground to the lowest and the two lowest $I^\pi = 4^+$ states in ^{20}Ne and ^{28}Si, respectively, are compared with the SCM predictions by Chung and Wildenthal (Ref. 63).

	Nucleus	^{20}Ne		^{28}Si			
	Method	PHM	SCM	PHM	SCM	PHM	SCM
	State no.	1	1	1	1	1	2
a	b \ ΔE (MeV)	4.23	4.13	3.23	5.29	7.70	7.90
$Os_{\frac{1}{2}}$	$Og_{\frac{9}{2}}$	0.0136		0.0148		+0.0036	
$Op_{\frac{1}{2}}$	$Of_{\frac{7}{2}}$	0.0660		0.0288		+0.0001	
$Op_{\frac{3}{2}}$	$Of_{\frac{5}{2}}$	−0.0740		−0.0383		−0.0002	
	$Of_{\frac{7}{2}}$	−0.0274		−0.0178		−0.0002	
$1s_{\frac{1}{2}}$	$Og_{\frac{9}{2}}$	−0.0784		−0.1035		−0.0097	
$Od_{\frac{3}{2}}$	$Od_{\frac{5}{2}}$	−0.5908	−0.6491	−0.6884	−1.0310	+0.6181	1.0373
	$Og_{\frac{9}{2}}$	0.0256		0.0895		−0.0030	
$Od_{\frac{5}{2}}$	$Od_{\frac{3}{2}}$	0.5224	0.5749	0.5601	0.5261	−0.3625	−0.3330
	$Od_{\frac{5}{2}}$	0.6732	0.8549	0.1909	0.0021	−0.0925	−0.4327
	$Og_{\frac{9}{2}}$	−0.0686		−0.0944		−0.0650	
$1p_{\frac{1}{2}}$	$Of_{\frac{7}{2}}$	−0.0085		−0.0115		−0.0001	
$1p_{\frac{3}{2}}$	$Of_{\frac{5}{2}}$	0.0063		0.0086		+0.0015	
	$Of_{\frac{7}{2}}$	0.0085		0.0080		−0.0009	
$Of_{\frac{5}{2}}$	$Op_{\frac{3}{2}}$	0.0974		0.0452		−0.0879	
	$1p_{\frac{3}{2}}$	−0.0059		−0.0088		−0.0069	
	$Of_{\frac{5}{2}}$	0.0238		0.0121		+0.0004	
	$Of_{\frac{7}{2}}$	−0.0205		−0.0117		+0.0030	
$Of_{\frac{7}{2}}$	$Op_{\frac{1}{2}}$	−0.0860		−0.0340		+0.0916	
	$Op_{\frac{3}{2}}$	−0.0299		−0.0207		+0.0481	
	$1p_{\frac{1}{2}}$	0.0053		0.0098		+0.0052	
	$1p_{\frac{3}{2}}$	0.0086		0.0075		+0.0027	
	$Of_{\frac{5}{2}}$	0.0211		0.0119		−0.0024	
	$Of_{\frac{7}{2}}$	0.0180		0.0144		−0.0023	
$Og_{\frac{9}{2}}$	$Os_{\frac{1}{2}}$	0.0139		0.0171		−0.0130	
	$1s_{\frac{1}{2}}$	−0.1421		−0.1487		+0.0413	
	$Od_{\frac{3}{2}}$	−0.0347		−0.1049		+0.0442	
	$Od_{\frac{5}{2}}$	−0.0998		−0.1077		+0.0827	
	$Og_{\frac{9}{2}}$	0.0104		−0.0010		+0.0024	

identical to the SCM values of Ref. 66. Once more, for ^{28}Si the agreement is worse. However, since the largest discrepancies occur here in those amplitudes which do not carry any magnetic strength, even in ^{28}Si a reasonable description of the magnetic dipole transitions within the PHM approach may still be expected.

With all these more or less encouraging results for the low excited states in mind we shall now turn our attention to the higher excited states in the region of the giant multipole resonances, which will be discussed one by one in the remaining part of this section.

A. The isoscalar electric monopole transitions ($E0S$)

The classical energy weighted sumrule (CEWSR) of Eq. (29) predicts total $E0S$ strengths of 2642 e^2fm^4 MeV for ^{20}Ne and 4628 e^2fm^4 MeV for ^{28}Si.

TABLE VII. The spectroscopic amplitudes (19) for the proton isovector magnetic dipole transitions from the ground to the strongest $I^\pi = 1^+$ states in ^{20}Ne and ^{28}Si are given and compared with the results of the SCM calculations by Chung and Wildenthal (Ref. 66).

	Nucleus	^{20}Ne		^{28}Si	
	Method	PHM	SCM	PHM	SCM
	State no.	1	1	3	3
a	ΔE (MeV) / b	9.72	11.29	11.21	13.28
$Os\frac{1}{2}$	$Os\frac{1}{2}$	0.0020		−0.0011	
	$1s\frac{1}{2}$	−0.0143		−0.0046	
	$Od\frac{3}{2}$	−0.0134		0.0183	
$Op\frac{1}{2}$	$Op\frac{1}{2}$	0.0013		−0.0017	
	$Op\frac{3}{2}$	−0.0012		−0.0030	
	$1p\frac{1}{2}$	0.0003		−0.0030	
	$1p\frac{3}{2}$	−0.0002		−0.0001	
$Op\frac{3}{2}$	$Op\frac{1}{2}$	−0.0057		0.0047	
	$Op\frac{3}{2}$	0.0003		0.0022	
	$1p\frac{1}{2}$	−0.0005		0.0004	
	$1p\frac{3}{2}$	0.0002		0.0003	
	$Of\frac{5}{2}$	−0.0007		0.0007	
$1s\frac{1}{2}$	$Os\frac{1}{2}$	−0.0085		0.0051	
	$1s\frac{1}{2}$	0.0554	0.0723	0.0712	0.0245
	$Od\frac{3}{2}$	0.0655	0.0306	−0.1434	−0.0698
$Od\frac{3}{2}$	$Os\frac{1}{2}$	−0.0000		0.0152	
	$1s\frac{1}{2}$	0.0913	0.0747	0.0271	0.2817
	$Od\frac{3}{2}$	−0.0780	−0.0698	−0.0729	−0.0980
	$Od\frac{5}{2}$	−0.0955	−0.1421	0.3727	0.4948
$Od\frac{5}{2}$	$Od\frac{3}{2}$	−0.2348	−0.2486	0.2784	0.2070
	$Od\frac{5}{2}$	−0.3653	−0.3686	0.1500	0.1543
$1p\frac{1}{2}$	$Op\frac{1}{2}$	−0.0029		0.0200	
	$Op\frac{3}{2}$	−0.0145		−0.0003	
	$1p\frac{1}{2}$	−0.0005		0.0020	
	$1p\frac{3}{2}$	−0.0029		0.0006	
$1p\frac{3}{2}$	$Op\frac{1}{2}$	0.0250		0.0011	
	$Op\frac{3}{2}$	0.0045		−0.0092	
	$1p\frac{1}{2}$	0.0029		0.0002	
	$1p\frac{3}{2}$	0.0026		−0.0009	
	$Of\frac{5}{2}$	0.0037		−0.0040	
$Of\frac{5}{2}$	$Op\frac{3}{2}$	−0.0094		0.0303	
	$1p\frac{3}{2}$	−0.0014		0.0026	
	$Of\frac{5}{2}$	0.0033		0.0002	
	$Of\frac{7}{2}$	0.0002		0.0006	
$Of\frac{7}{2}$	$Of\frac{5}{2}$	0.0031		−0.0033	
	$Of\frac{7}{2}$	0.0039		−0.0017	
$Og\frac{9}{2}$	$Og\frac{9}{2}$	−0.0042		0.0016	

As can be seen from Table VIII, the calculations with the harmonic oscillator representation for the monopole transition operator (HO) give only 31% and 30% of these classical predictions, respectively. The use of the more realistic Woods-Saxon basis (WS), yielding 39% of the CEWSR for ^{20}Ne and 32% for ^{28}Si, does not increase these values considerably.

As already discussed above, a couple of the low excited isoscalar 0^+ states in both nuclei considered are of many particle many hole structure with respect to the dominant component of the corresponding ground state and cannot be reproduced within our truncated configuration space. However, since these states are at low excitation energies and do not connect strongly to the ground state via a one body operator because of their complicated structure, they would yield only minor contributions to the $E0S$ sumrule. The missing strength therefore has to be attributed almost entirely to the truncation of the single particle basis. In fact, with the $1s0d$ shell being partly occupied in both nuclei considered, large contributions to the transition strength are expected from the $2\hbar\omega$ 1p1h excitations into the $2s$ and $1d$ orbits of the $2s1d0g$ shell, which have not been included in our single particle basis. Because of the larger r^2 matrix element and the higher single particle angular momentum involved, for example, the $0d_{\frac{5}{2}}$ to $1d_{\frac{5}{2}}$ monopole excitations should carry considerably more transition strength than the $0p$ to $1p$ particle-hole configurations, which are explicitly taken into account here. It is therefore easily understood why we obtain only about 30% of the CEWSR in our calculations. Nevertheless, we think that the neglect of the $2s$ and $1d$ orbits in the present calculations is justified for the following reason. If calculated with a reasonable Woods-Saxon potential (i.e., one with not too unrealistic parameters), all the neglected orbits turn out to be high up in the continuum, none of them showing any single particle resonance behavior. Consequently, these orbits have to be attributed with very large widths and hence any transition strength resulting from particle-hole excitations into them will be spread over a large energy interval. At least with the present experimental techniques such widely spread strength can hardly be disentangled from the usual background seen, for example, in inelastic α-scattering measurements. Therefore, we would conclude, if any concentrated $E0S$ strength exhausting a considerable portion of the CEWSR can be localized at all experimentally in the two nuclei considered here, it most probably should be attributed to those configurations which are taken into account explicitly in the present calculations. This argument gets some additional support from the fact that the

TABLE VIII. Total calculated energy weighted strengths for the electromagnetic transitions of various multipolarities in the two nuclei considered as obtained using either the harmonic oscillator (HO) or the Woods-Saxon (WS) representation of the transition operators. For the electric transitions, the strengths are given in percent of the corresponding classical energy weighted sum rules; for the magnetic ones, the absolute calculated values are displayed. In the case of the nearly pure isovector magnetic operators, the isoscalar strengths are given in percent of the corresponding calculated isovector strengths.

Nucleus		^{20}Ne		^{28}Si	
Radial wave functions		HO	WS	HO	WS
$E0$	$T=0$	31%	39%	30%	32%
	$T=1$	60%	58%	54%	44%
$E1$	$T=1$	84%	86%	106%	100%
$E2$	$T=0$	55%	45%	61%	54%
	$T=1$	84%	66%	96%	83%
$E3$	$T=0$	27%	38%	33%	43%
	$T=1$	57%	74%	65%	85%
$E4$	$T=0$	41%	93%	40%	68%
	$T=1$	50%	103%	51%	84%
$M1$	$T=0$	0.2% ($T=1$)	0.2% ($T=1$)	0.3% ($T=1$)	0.3% ($T=1$)
($\mu_K{}^2$ MeV	$T=1$	38.0	40.0	68.0	68.0
$M2$	$T=0$	5% ($T=1$)	5% ($T=1$)	6% ($T=1$)	6% ($T=1$)
($\mu_K{}^2$fm^2 MeV)	$T=1$	2.9×10^5	3.0×10^5	5.3×10^5	5.0×10^5
$M3$	$T=0$	5% ($T=1$)	5% ($T=1$)	5% ($T=1$)	6% ($T=1$)
($\mu_K{}^2$fm^4 MeV)	$T=1$	1.3×10^6	9.4×10^5	2.8×10^6	2.5×10^6

monopole strength associated with the included configurations will already be spread over a considerable energy interval due to the relatively large widths of the $1p$ orbits.

Though yielding rather similar fractions of the CEWSR in both nuclei considered, the HO and the WS bases produce drastically different strength distributions. In ^{20}Ne, for example, the HO representation of the transition operator concentrates almost all the calculated $E0S$ strength into just two states; one at 17.83 MeV excitation energy, carrying 18.8%, and the second at 22.11 MeV, exhausting 6.4% of the CEWSR (upper left of Fig. 3). A similar result is observed for ^{28}Si; here 17.5% and 6.9% of the CEWSR are represented by the two states at 19.78 and 22.06 MeV, respectively (upper left of Fig. 4). If now, instead of the HO, the more realistic WS wave functions are used, these distributions are drastically changed. In both nuclei (^{20}Ne; upper right of Fig. 3; ^{28}Si; upper right of Fig. 4) the $E0S$ strength is distributed over a much larger energy interval and its center of gravity is shifted to higher excitation energies. In ^{20}Ne, for example, the 17.83 MeV state now exhausts only 6.4%, the 22.11 MeV state only 1.5% of the CEWSR. Instead, the two states at 24.23 and 29.19 MeV carrying only 1.5% and 1.2% of the CEWSR in the HO representation, are now participating with 8.4% and 5.5% of the classical strength, respectively. Similarly, the strength of the 19.78 MeV state in ^{28}Si is reduced from 17.5% (HO) to only 4% (WS), and that of the 29.63 MeV state in the same nucleus is increased from 1.3% (HO) to 8.5% (WS) of the CEWSR.

The reason for these drastic redistributions of the $E0S$ strengths due to the change of the single particle wave functions in the two nuclei considered can be understood from Tables IX and X, where the monopole transitions to some of the above mentioned states are analyzed in more detail. Let us first consider the 17.86 MeV state in ^{20}Ne (Table IX). As can be seen from the proton spectroscopic amplitudes S (19) presented in the second column of the table, the dominant spheri-

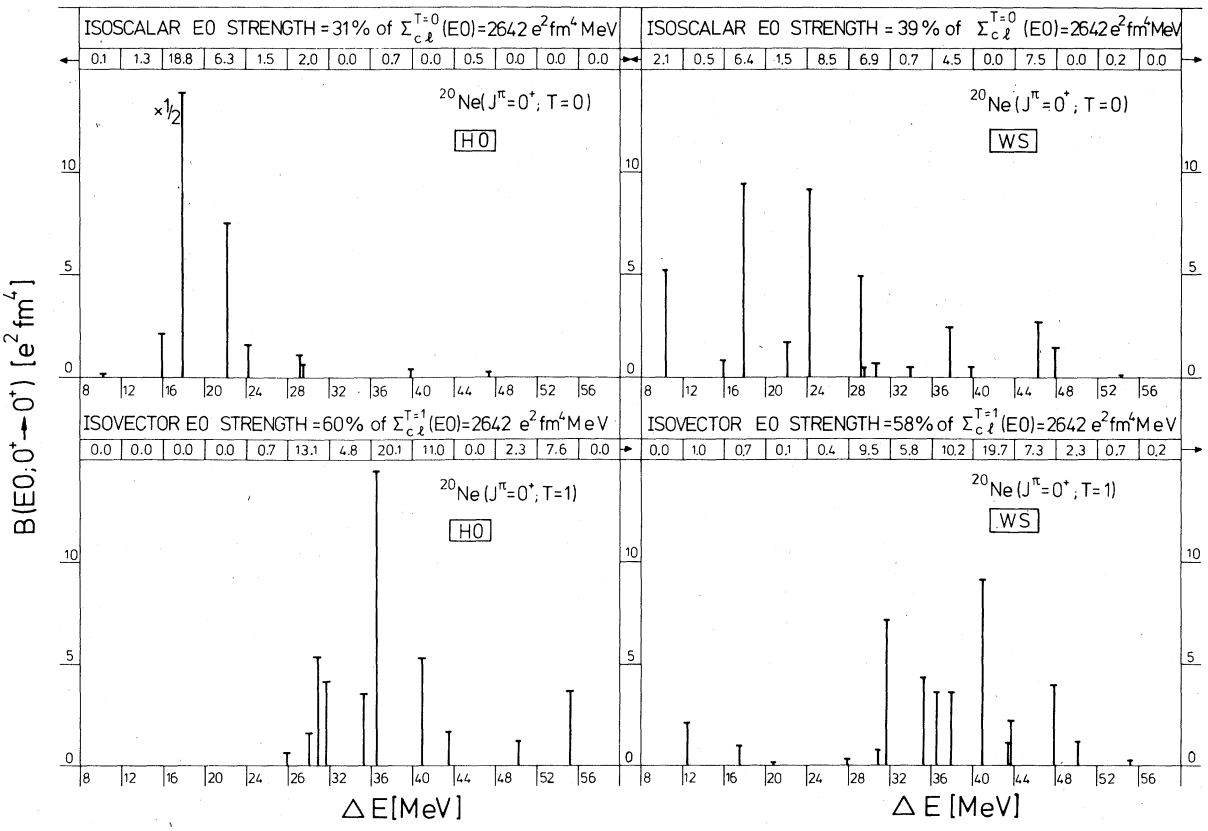

FIG. 3. The calculated isoscalar and isovector monopole transitions in ^{20}Ne are given and the results obtained with the oscillator and the Woods-Saxon single particle basis are compared. All the $B(E0)$ values are given in (e^2fm^4). In addition the figure presents the theoretical strength distributions obtained in the various energy intervals as a percentage of the corresponding classical energy weighted sum rule. Arrows indicate that strength above (or below) the energy limits shown in the plots has been included in the last (or first) energy interval.

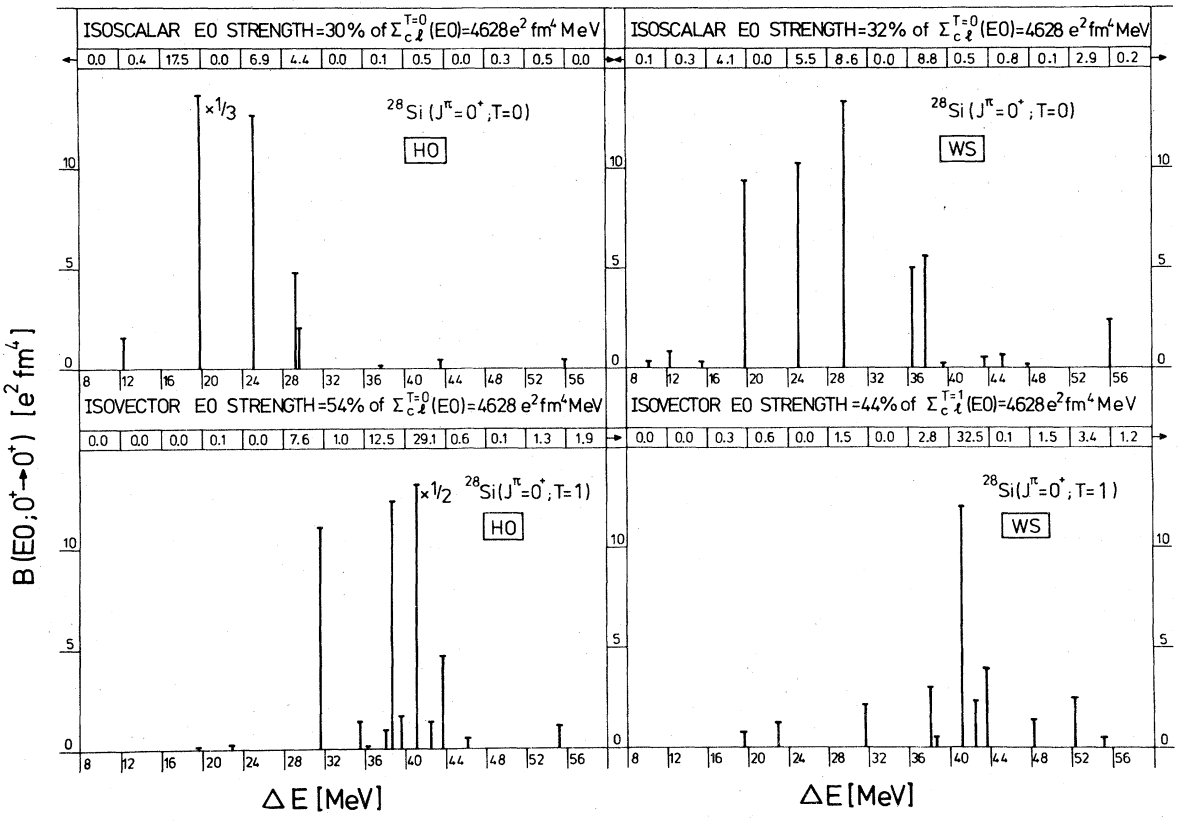

FIG. 4. Same as in Fig. 3 for the nucleus ^{28}Si.

cal components of this state are the 1p-0p particle-hole excitations. Multiplying these spectroscopic amplitudes now with the reduced $E0$ single particle transition matrix elements, we obtain a decomposition of the total transition amplitude (22) into its individual components. As expected because of the dissimilarity of the WS 1p orbits with the corresponding HO levels, the 1p-0p components of the transition amplitude are reduced if the HO are replaced by the WS wave functions. However, this reduction is only moderate. The drastic change in the total transition amplitude is essentially due to the large increase of the diagonal $1p_{\frac{1}{2}}$-$1p_{\frac{1}{2}}$ and $1p_{\frac{3}{2}}$-$1p_{\frac{3}{2}}$ terms, which because of their opposite sign cancel part of the 1p-0p particle-hole contributions and hence lead to a large reduction of the transition amplitude. For the 24.23 MeV transition these large diagonal recoupling terms, which describe a redistribution of the particles inside the 1p shell relative to the ground state, are even responsible for a sign change of the total amplitude, and again the same effect leads to an increase of the monopole transition strength to the 29.19 MeV in ^{20}Ne. Similar effects are observed in ^{28}Si (Table X). Depending on the relative signs of the spectroscopic amplitudes S, here also the strongly increasing diagonal 1p terms yield reduced (for the 19.78 MeV state), increased (for the 29.63 MeV level), or sometimes almost unchanged (for the 25.06 MeV state) total transition amplitudes if the HO wave functions are replaced by the more realistic WS basis.

Thus it becomes evident that for a proper description of the isoscalar electric monopole states the choice of suitable single particle wave functions is rather essential. Considering the WS basis as more realistic than the HO one, one has to conclude that the $E0S$ strength in ^{20}Ne as well as in ^{28}Si is very likely spread over many states in a large energy interval with no single level exhausting more than about 9% of the CEWSR. Additionally taking into account that even this small amount of monopole transition strength in reality will be considerably smeared out due to the large widths of the 1p orbits, it becomes rather unlikely that any remarkable amount of $E0S$ strength can be experimentally localized at all in the two nuclei considered here. This conclusion, which would not be affected even if ambiguities of 2 or 3 MeV in the excitation energies of the individual states due to our assumption of a constant correlation energy are admitted, is in perfect agreement with

TABLE IX. The spectroscopic amplitudes (19) for the proton isoscalar electric monopole transitions from the ground state to some selected $I^\pi = 0^+$ states in ^{20}Ne are given as well as the corresponding transition amplitudes (22) obtained with the harmonic oscillator (HO) as well as the Woods-Saxon (WS) representations of the transition operator.

ΔE (MeV)			17.86			24.23			29.19	
$B(E0)$ (e^2fm^4)			27.78	9.47		1.60	9.11		1.08	4.97
% of $\Sigma_{cl}^{T=0}(E0)$			18.8	6.4		1.5	8.4		1.2	5.5
p	h	S	T (HO)	T (WS)	S	T (HO)	T (WS)	S	T (HO)	T (WS)
$0s\frac{1}{2}$	$0s\frac{1}{2}$	−0.010	−0.061	−0.064	0.019	0.111	0.118	−0.005	−0.028	−0.030
	$1s\frac{1}{2}$	−0.000	0.001	0.001	−0.010	0.048	0.049	0.000	−0.000	−0.000
$0p\frac{1}{2}$	$0p\frac{1}{2}$	−0.010	−0.103	−0.104	0.088	0.872	0.882	0.041	0.415	0.420
	$1p\frac{1}{2}$	−0.003	0.021	0.020	0.009	−0.058	−0.055	0.004	−0.024	−0.022
$0p\frac{3}{2}$	$0p\frac{3}{2}$	−0.020	−0.279	−0.286	0.081	1.136	1.166	0.002	0.035	0.036
	$1p\frac{3}{2}$	−0.005	0.049	0.046	0.013	−0.111	−0.105	−0.000	0.003	0.003
$1s\frac{1}{2}$	$0s\frac{1}{2}$	0.047	−0.229	−0.232	−0.077	0.375	0.379	0.022	−0.106	−0.107
	$1s\frac{1}{2}$	0.012	0.165	0.239	0.046	0.643	0.935	0.008	0.111	0.161
$0d\frac{3}{2}$	$0d\frac{3}{2}$	0.031	0.602	0.750	−0.024	−0.476	−0.593	0.017	0.325	0.406
$0d\frac{5}{2}$	$0d\frac{5}{2}$	−0.024	−0.579	−0.633	−0.014	−0.348	−0.380	−0.012	−0.288	−0.315
$1p\frac{1}{2}$	$0p\frac{1}{2}$	0.255	−1.601	−1.498	−0.125	0.787	0.736	0.026	−0.166	−0.155
	$1p\frac{1}{2}$	0.026	0.468	1.192	−0.019	−0.336	−0.857	−0.008	−0.150	−0.382
$1p\frac{3}{2}$	$0p\frac{3}{2}$	0.436	−3.873	−3.661	−0.228	2.026	1.915	0.042	−0.377	−0.357
	$1p\frac{3}{2}$	0.069	1.745	4.190	−0.047	−1.176	−2.823	−0.012	−0.314	−0.754
$0f\frac{5}{2}$	$0f\frac{5}{2}$	−0.021	−0.662	−1.501	−0.037	−1.138	−2.580	−0.016	−0.490	−1.111
$0f\frac{7}{2}$	$0f\frac{7}{2}$	−0.024	−0.863	−1.395	−0.027	−0.966	−1.563	0.004	0.144	0.234
$0g\frac{9}{2}$	$0g\frac{9}{2}$	−0.001	−0.072	−0.140	−0.003	−0.125	−0.244	−0.003	−0.130	−0.253
ΣT (e fm^2)			−5.271	−3.077		1.264	−3.018		−1.040	−2.229

the present experimental situation; in fact, up to now in nuclei below ^{40}Ca no experimental evidence for concentrated electric monopole strengths exhausting more than a few percent of the CEWSR has been found.[20]

B. The isovector electric monopole transitions ($E0V$)

The CEWSR of Eq. (29) predicts for the $E0V$ transitions the same total strength as for the isoscalar monopole states. On the other hand, as can be seen from Table VIII, our calculations obtain here a considerably larger portion of this classical prediction than in the latter case. In ^{20}Ne the PHM results exhaust 60% (HO) and 58% (WS) of the classical $E0V$ sumrule, and in ^{28}Si the corresponding values are 54% (HO) and 44% (WS). Since in the calculations for the $E0V$ states the same configuration spaces as for the $E0S$ levels have been used, this result suggests a strong velocity dependence of our Hamiltonian, because, as already mentioned in the last section, such velocity dependent terms in the interaction are not taken into account by the CEWSR. Whether this strong velocity dependence of our microscopic Hamiltonian is reasonable or not unfortunately cannot be judged, since up to now, neither in heavy nor in light nuclei, no isovector electric monopole resonances have been found experimentally and hence no data for comparison are available.

The $E0V$-strength distributions obtained for ^{20}Ne and ^{28}Si are displayed in the lower parts of Figs. 3 and 4, respectively. As expected from the isospin dependence of the nuclear interaction, the $E0V$ strength occurs at considerably larger excitation energies than the $E0S$ one. Again, as in the case of the $E0S$ transitions, the use of WS instead of HO wave functions broadens the distributions and shifts their center of gravity to somewhat higher excitation energies. Since the $E0V$ strength is in both nuclei distributed over many individual

TABLE X. Same as in Table IX, but for some selected isoscalar electric monopole states in ^{28}Si.

ΔE (MeV)			19.78			25.06			29.63	
$B(E0)$ (e^2fm^4)			40.99	9.36		12.67	10.21		2.05	13.31
% of $\Sigma_{cl}^{T=0}(E0)$			17.5	4.0		6.9	5.5		1.3	8.5
p	h	S	T (HO)	T (WS)	S	T (HO)	T (WS)	S	T (HO)	T (WS)
$Os\frac{1}{2}$	$Os\frac{1}{2}$	−0.004	−0.024	−0.026	0.003	0.022	0.024	−0.004	−0.023	−0.026
	$1s\frac{1}{2}$	−0.006	0.030	0.031	0.004	−0.023	−0.024	0.002	0.012	−0.013
$Op\frac{1}{2}$	$Op\frac{1}{2}$	0.000	0.002	0.002	−0.004	−0.047	−0.046	−0.048	−0.530	−0.520
	$1p\frac{1}{2}$	−0.001	0.005	0.005	−0.000	0.001	0.001	−0.004	0.027	0.024
$Op\frac{3}{2}$	$Op\frac{3}{2}$	−0.003	−0.046	−0.046	0.018	0.282	0.286	−0.059	−0.914	−0.925
	$1p\frac{3}{2}$	−0.001	0.013	0.010	0.002	−0.022	−0.018	−0.007	0.068	0.054
$1s\frac{1}{2}$	$Os\frac{1}{2}$	0.018	−0.097	−0.100	−0.014	0.074	0.076	0.010	−0.054	−0.056
	$1s\frac{1}{2}$	0.020	0.308	0.336	−0.024	−0.369	−0.402	−0.015	−0.224	−0.244
$Od\frac{3}{2}$	$Od\frac{3}{2}$	0.023	0.510	0.509	−0.020	−0.428	−0.427	−0.012	−0.255	−0.254
$Od\frac{5}{2}$	$Od\frac{5}{2}$	−0.025	−0.654	−0.651	0.026	0.685	0.682	0.007	0.192	0.191
$1p\frac{1}{2}$	$Op\frac{1}{2}$	0.224	−1.559	−1.386	−0.424	2.951	2.624	0.096	−0.665	−0.591
	$1p\frac{1}{2}$	0.013	0.250	0.499	−0.036	−0.706	−1.409	0.026	0.508	1.013
$1p\frac{3}{2}$	$Op\frac{3}{2}$	0.488	−4.799	−3.849	−0.078	0.763	0.612	−0.070	0.688	0.552
	$1p\frac{3}{2}$	0.048	1.336	3.917	0.011	0.308	0.903	0.012	0.343	1.006
$Of\frac{5}{2}$	$Of\frac{5}{2}$	−0.016	−0.544	−0.885	0.009	0.297	0.483	0.023	0.773	1.257
$Of\frac{7}{2}$	$Of\frac{7}{2}$	−0.024	−0.964	−1.079	−0.008	−0.321	−0.360	0.025	0.975	1.092
$Og\frac{9}{2}$	$Og\frac{9}{2}$	−0.003	−0.170	−0.345	0.002	0.094	0.191	0.010	0.536	1.087
ΣT (e fm^2)			−6.403	−3.059		3.561	3.196		1.433	3.648

states, each of which (again the dominant spherical components are the 1p-0p excitations) has to be attributed with a considerably large width, one expects a rather flat $E0V$-strength distribution between excitation energies of about 25 and 55 MeV in both ^{20}Ne and ^{28}Si. As for the $E0S$ transitions, here also there is not very much hope that these extremely broad distributions could be detected with the present experimental techniques.

C. The isoscalar magnetic dipole transitions ($M1V$)

In contrast to the electric monopole transitions, where drastic changes of the results were obtained, if the HO was replaced by the WS basis, for the $M1V$ transitions both sets of single particle wave functions yield nearly identical results. This is easily understood from the fact that the $M1$ transition operator has no radial dependence and hence the only difference in the WS single particle $M1$ matrix elements with respect to the HO ones is caused by the small differences in the radial wave functions of spin-orbit partners induced by the spin-orbit term of the WS potential.

In ^{20}Ne inelastic electron scattering measurements under 180° scattering angle[9] detect only one single state with a strong magnetic dipole transition: the isovector 1^+ level at 11.235 MeV with a $B(M1; 0^+ \rightarrow 1^+)$ value of $2.06 \pm 0.36\ \mu_K^2$. As can be seen from the upper half of Fig. 5, the PHM approach also concentrates nearly all the $M1V$ strength in ^{20}Ne into a single state, predicting an excitation energy of 9.72 MeV and a $B(M1)$ value of $1.59\ \mu_K^2$. As already discussed above, the $L^\pi = 1^+$ proton spectroscopic amplitudes for this transition agree surprisingly well with the predictions of Chung and Wildenthal's SCM calculation.[66] Since, furthermore, the 1.5 MeV discrepancy in the excitation energy can be easily attributed to the ambiguity introduced by our assumption of a constant correlation energy, we consider this result rather satisfying; even more so since it was obtained in a completely microscopic calculation with no fitted effective interaction and g factor at all.

In ^{28}Si (see the upper half of Fig. 6) the old electron scattering data of Fagg *et al.*[8] show one

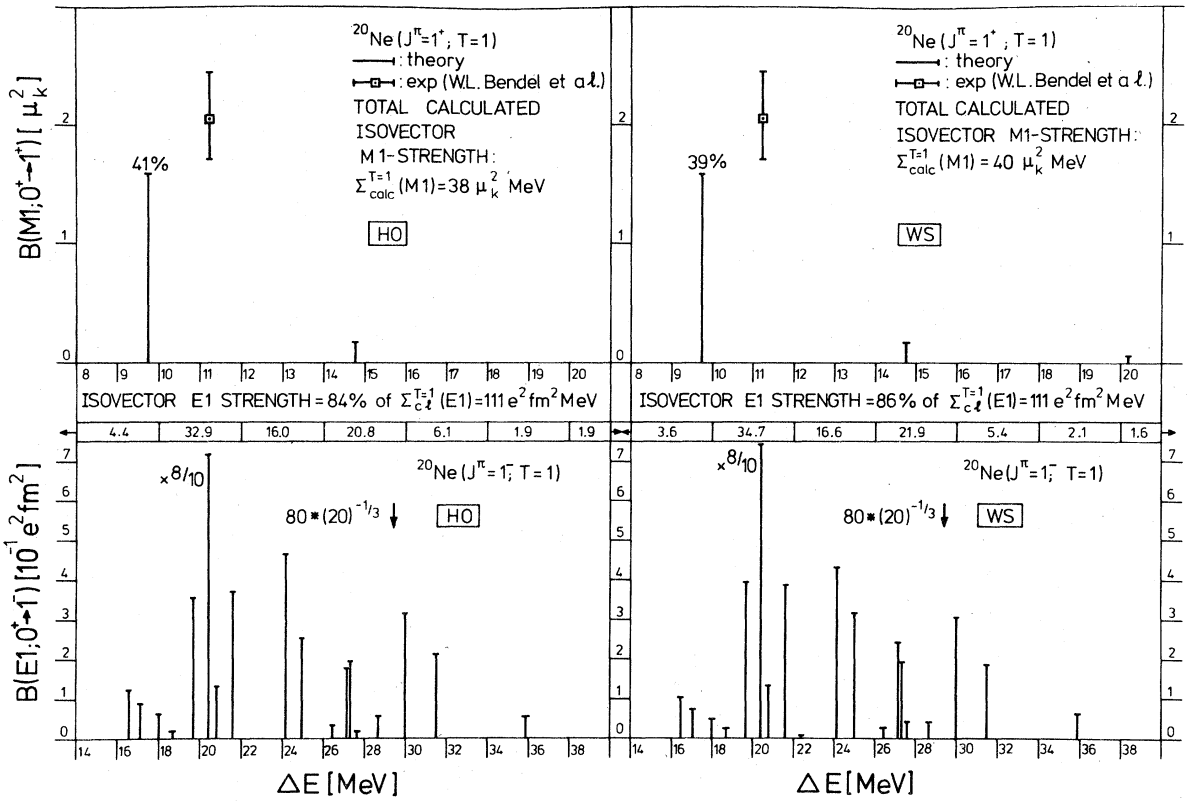

FIG. 5. The calculated isovector magnetic and electric dipole transitions in ^{20}Ne are given. Again the results obtained with the oscillator basis are compared to those obtained with the Woods-Saxon single nucleon functions. The $B(M1;0^+\rightarrow 1^+)$ values are given in units of (μ_K^2), the $B(E1;0^+\rightarrow 1^-)$ values in $(10^{-1}e^2\mathrm{fm}^2)$. The measured $M1$ strength has been taken from Ref. 9. In the case of the $E1$ transitions, again the strength distribution is given as a percentage of the classical energy weighted isovector $E1$ sumrule. The arrow at $80\,(20)^{-1/3}$ MeV indicates the classical position of the giant dipole resonance.

strong $M1$ transition at 11.41 MeV and a few smaller ones around this excitation energy, adding up to a total nonenergy weighted $M1V$ strength of 6.79 (+1.97, −1.61) μ_K^2. Recent high resolution experiments performed at Darmstadt by Schneider *et al.*[21] improved this value to 5.82 ± 0.24 μ_K^2 but confirm the overall features of the older data. Here also one strong $M1$ transition [now at 11.45 MeV with an about 10% larger $B(M1)$ value than the old data] and a few satellites [with about 20–40% smaller $B(M1)$'s than in Fagg's experiment] are found. Though reproducing the qualitative features of this experimental $M1V$-strength distribution reasonably well, the PHM approach here fails to predict the full experimental sumrule and obtains only 4.12 μ_K^2 below 20 MeV excitation energy. This failure most probably has to be attributed to our microscopic Hamiltonian and not to the configuration space, since also in 1s0*d* shell SCM calculations, which for some effective interactions obtain almost perfect agreement with the experimental value [6.47 μ_K^2 (Ref. 21); 5.92 μ_K^2 (Ref. 54)], a similar lack of strength is observed, if forces like the Kuo interaction[51] (which like our Hamiltonian is based on the Hamada-Johnston potential[49]) are used.[67]

Thus one has to admit that the PHM approach does not reproduce the experimental data for the $M1V$ transitions as well as the SCM model. However, from a large basis calculation with a microscopic Hamiltonian this could not be expected. Nevertheless, the qualitative features of the experimental $M1V$-strength distributions are reasonably well reproduced.

Finally, we would like to mention that because of the anomalous magnetic moment of the neutron, the magnetic dipole operator is an almost pure isovector operator. Therefore, as can be seen from Table VIII, the isoscalar $M1$ transitions in both nuclei considered here carry less than 0.3% of the corresponding energy weighted $M1V$ strength and will not be discussed in the present paper.

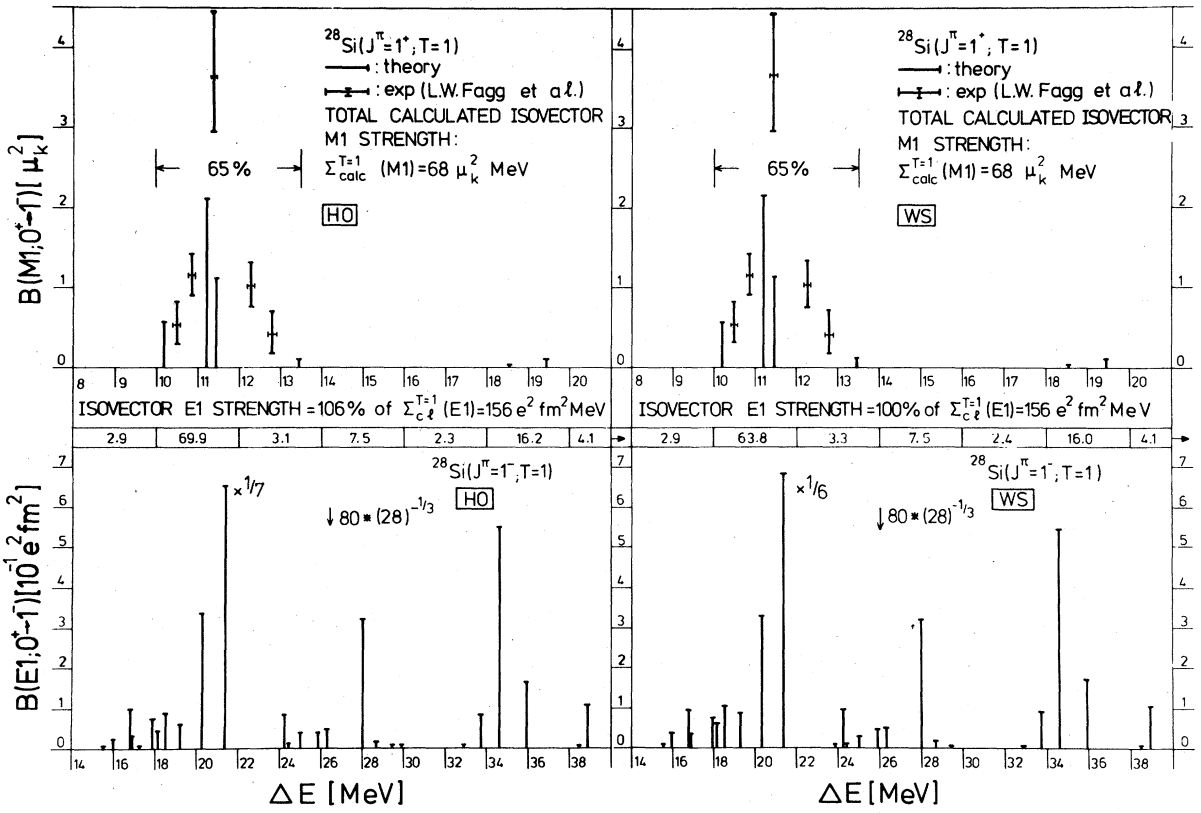

FIG. 6. Same as in Fig. 5 for the nucleus ^{28}Si. The measured $M1$ transitions have been taken from Ref. 8.

D. The isovector electric dipole transitions ($E1V$)

The strength distributions obtained for the $E1V$ transitions in ^{20}Ne and ^{28}Si are displayed in the lower halves of Figs. 5 and 6, respectively. Depending only linearly on r, the electric dipole operator is not very sensitive to changes in the radial dependence of the single particle wave functions. Therefore, for the magnetic dipole transitions, here also the HO and the WS bases yield very similar results and hence need not be discussed separately in the following.

Comparing the $E1V$-strength distributions for the two nuclei, one essential difference becomes immediately evident: While in ^{20}Ne the electric dipole strength is spread over many states between 16 and 32 MeV excitation energy, in ^{28}Si nearly 70% of the total energy weighted $E1V$ strength is concentrated into two single levels; one at 21.37 MeV, the other at 34.59 MeV excitation energy. Analysis of the corresponding $L^\pi = 1^-$ spectroscopic amplitudes shows that the strong dipole excitation at 21.37 MeV (as well as its nearest neighbor) is essentially a coherent superposition of sd to pf particle-hole excitations, while the 34.59 MeV state (as well as the relatively large transition at 28 MeV) is of almost pure p to sd particle-hole structure.

In ^{20}Ne, on the other hand, nearly all the states displayed in Fig. 5 are mixtures of these two different modes of $1\hbar\omega$ excitations. The reason for this different structure of the electric dipole states in the two nuclei can be understood from the intrinsic HF single particle energy spectra (Fig. 1), which have already been discussed in the last section. In ^{20}Ne, the average energy gaps between the occupied $0p$ and empty $1s0d$ levels and between the occupied $1s0d$ and empty $1p0f$ orbits is of about the same size. Consequently, the two modes of excitation are strongly competing and the resulting isovector 1^- states are strongly mixed. In ^{28}Si, the $1s0d$ to $1p0f$ excitations are considerably favored in energy with respect to the $0p$ to $1s0d$ particle-hole states. Therefore here the two excitation modes are energetically well separated and the resulting dipole states represent almost entirely either one or the other of them.

Experimentally, the most valuable information about the electric dipole resonances in the two nuclei considered here are most probably those obtained by proton radiative capture reactions on

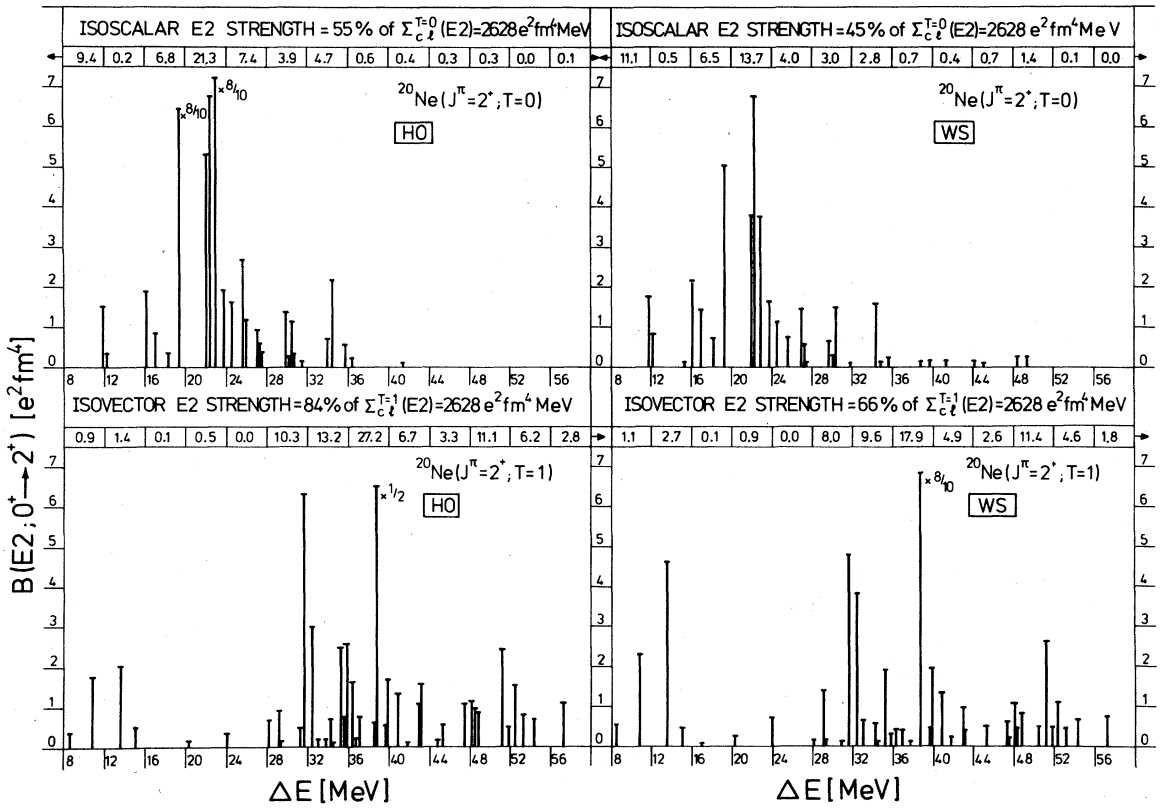

FIG. 7. The isoscalar and isovector electric giant quadrupole resonances as calculated for ^{20}Ne. The results of calculations using the oscillator basis and the Woods-Saxon Basis are compared. In addition the figure displays the strength distributions as a percentage of the corresponding classical energy weighted sum rule. The classical predictions for the positions of the isoscalar and isovector $E2$ resonance are about 23 and 44 MeV, respectively. All $B(E2; 0^+ \rightarrow 2^+)$ values are in units of $(e^2\text{fm}^4)$.

the neighboring odd A nuclei ^{19}F(Ref. 7) and ^{27}Al,[6] respectively. Unfortunately, as has been shown, for example, in Refs. 33, the $E1V$-strength distributions presented here cannot be compared directly with the experimental (p,γ) cross sections. For example, unlike inelastic α scattering which excites all the isoscalar natural parity states that are connected to the target ground state with large enough $B(EL)$ values, the (p,γ) process selects only particular components of the GMR's and therefore tests only specific parts of the total strength distributions. Depending strongly on the structure of the target ground state (only $p_{\frac{1}{2}}$ and $p_{\frac{3}{2}}$ proton waves can form a 1^- excitation together with the $\frac{1}{2}^+$ ground state of ^{19}F, while $p_{\frac{3}{2}}$, $f_{\frac{5}{2}}$, and $f_{\frac{7}{2}}$ waves can couple to this total spin value with the $\frac{5}{2}^+$ ground state of ^{27}Al), the (p,γ) entrance channel favors only some components of the 1^- wave functions and supresses the others. Consequently, the resulting cross section may look rather different from the predictions for the $E1V$ distributions presented here. Furthermore, for a large enough 1^- level density, the individual states will interact with each other via the propagator of the (p,γ) T matrix, an effect which may again yield a redistribution of the transition strength as well as considerable shifts in the excitation energies.[33] In the present work we shall therefore restrict ourselves to only some qualitative comparisons.

In the experimental ^{19}F (p,γ) ^{20}Ne cross section, as in our calculations, the $E1V$ strength is distributed over many levels between about 16 and 25 MeV excitation energy. The main theoretical contribution is about 1 to 2 MeV higher excitation energy than seen in experiment. Since part of this discrepancy may be explained by the level shifts to be expected from a proper treatment of

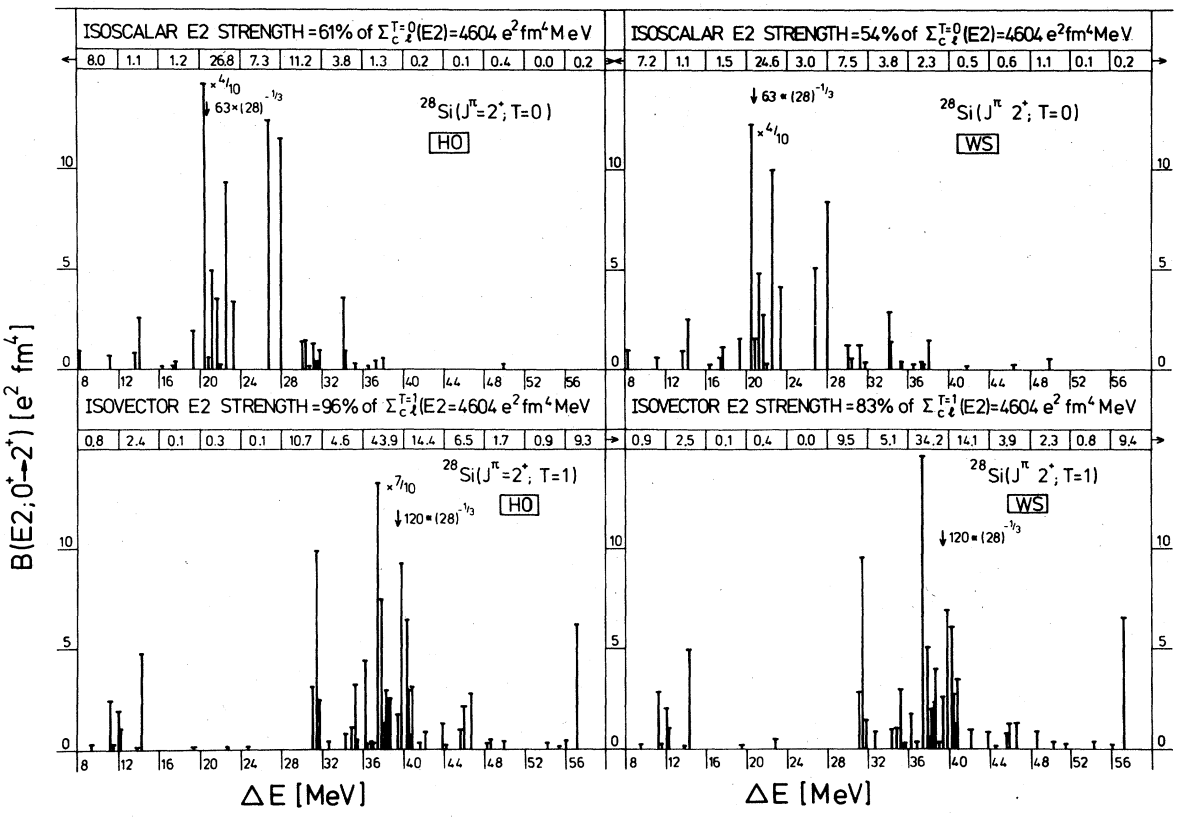

FIG. 8. Same as in Fig. 7, but for the nucleus ^{28}Si. Here the classical predictions for the positions of the resonances are indicated by arrows.

the continuum-bound state coupling, and the rest can be easily attributed to the ambiguity introduced by the constant correlation energy, the qualitative agreement with the experimental data is, for a completely microscopic calculation, still rather satisfying. Similar conclusions may be drawn for ^{28}Si. Also here the theory predicts the main $E1V$ contributions in the right energy region. However, in contrast to ^{20}Ne, where the spin projected 1p1h configurations (17) already yield a sufficient spreading of the $E1V$ strength in the relevant energy region, in ^{28}Si the strong concentration of $E1V$ strength in the 21.37 MeV level seems to indicate that some additional spreading due to the coupling to more complicated configurations than included here may be required to give a quantitative description of the experimental data.

Finally we would like to point out that with respect to electric dipole excitations, our configuration spaces are almost complete. Therefore, as can be seen from Table VIII, the PHM approach here obtains 85% and 100% of the CEWSR (31) for ^{20}Ne and ^{28}Si, respectively. However, note that we have introduced an enhancement factor of $\chi = 0.5$ CEWSR, which is perhaps somewhat too large for nuclei in the *sd*-shell mass region. If that is true, then in ^{28}Si the calculations would even overestimate the CEWSR, indicating that either the PHM approach does not yield enough ground state correlations for this nucleus, or that our microscopic Hamiltonian contains velocity dependent terms which are to strong. However, since nobody really knows the right value of χ for the nuclei considered here, we shall not speculate on this point any further.

E. The isoscalar electric quadrupole transitions ($E2S$)

The CEWSR of Eq. (30) predicts total $E2S$ strengths of 2628 e^2 fm^4 MeV for ^{20}Ne and 4604 e^2 fm^4 MeV for ^{28}Si. As can be seen from

TABLE XI. The spectroscopic amplitudes (19) for the proton isoscalar electric quadrupole transitions from the ground state to some selected $I^\pi = 2^+$ states in ^{20}Ne are given as well as the corresponding transition amplitudes (22) calculated with harmonic oscillator (HO) as well as with Woods-Saxon (WS) single nucleon wave functions.

ΔE (MeV)			22.34			22.89	
$B(E2)$ (e^2fm^4)			8.45	6.78		9.02	3.77
% of $\Sigma_{cl}^{T=0}(E2)$			7.2	5.8		7.9	3.3
p	h	S	T (HO)	T (WS)	S	T (HO)	T (WS)
$0s\frac{1}{2}$	$0d\frac{3}{2}$	0.005	0.017	0.017	−0.003	−0.009	−0.009
	$0d\frac{5}{2}$	−0.007	−0.024	−0.026	0.003	0.010	0.010
$0p\frac{1}{2}$	$0p\frac{3}{2}$	0.028	0.110	0.112	−0.035	−0.139	−0.142
	$1p\frac{3}{2}$	0.005	−0.013	−0.012	−0.006	0.014	0.014
	$0f\frac{5}{2}$	0.005	0.028	0.024	−0.006	−0.036	−0.030
$0p\frac{3}{2}$	$0p\frac{1}{2}$	−0.015	0.060	0.061	0.086	−0.341	−0.347
	$0p\frac{3}{2}$	−0.042	0.166	0.171	0.029	−0.113	−0.116
	$1p\frac{1}{2}$	−0.001	−0.003	−0.002	0.010	0.026	0.023
	$1p\frac{3}{2}$	−0.007	−0.017	−0.016	0.004	0.011	0.010
	$0f\frac{5}{2}$	0.006	0.018	0.015	−0.003	−0.009	−0.007
	$0f\frac{7}{2}$	0.007	0.051	0.051	−0.003	−0.022	−0.022
$1s\frac{1}{2}$	$0d\frac{3}{2}$	−0.022	0.111	0.151	0.014	−0.071	−0.096
	$0d\frac{5}{2}$	0.030	−0.185	−0.223	−0.006	0.034	0.041
$0d\frac{3}{2}$	$0s\frac{1}{2}$	−0.126	0.386	0.400	0.114	−0.349	−0.362
	$1s\frac{1}{2}$	0.107	0.537	0.731	0.027	0.138	0.187
	$0d\frac{3}{2}$	0.046	−0.254	−0.317	0.064	−0.353	−0.440
	$0d\frac{5}{2}$	−0.122	−0.443	−0.509	0.007	0.024	0.028
$0d\frac{5}{2}$	$0s\frac{1}{2}$	0.109	0.411	0.431	−0.148	−0.556	−0.583
	$1s\frac{1}{2}$	0.067	−0.411	−0.495	−0.071	0.438	0.527
	$0d\frac{3}{2}$	−0.030	0.109	0.126	−0.016	0.057	0.066
	$0d\frac{5}{2}$	0.008	−0.059	−0.065	−0.017	0.126	0.138
	$0g\frac{9}{2}$	0.013	0.154	0.118	−0.007	−0.079	−0.061
$1p\frac{1}{2}$	$0p\frac{3}{2}$	−0.085	0.212	0.191	0.258	−0.646	−0.582
	$1p\frac{3}{2}$	−0.013	−0.095	−0.186	0.055	0.391	0.764
	$0f\frac{5}{2}$	−0.009	0.064	0.015	−0.031	0.222	0.053
$1p\frac{3}{2}$	$0p\frac{1}{2}$	0.101	0.254	0.244	−0.174	−0.436	−0.419
	$0p\frac{3}{2}$	−0.213	−0.534	−0.505	−0.471	−1.179	−1.114
	$1p\frac{1}{2}$	0.011	−0.079	−0.155	−0.030	0.214	0.419
	$1p\frac{3}{2}$	−0.046	0.329	0.790	−0.097	0.689	1.653
	$0f\frac{5}{2}$	−0.031	0.119	0.202	−0.016	0.063	0.106
	$0f\frac{7}{2}$	−0.001	0.005	0.009	−0.019	0.183	0.332
$0f\frac{5}{2}$	$0p\frac{1}{2}$	0.489	2.805	2.395	−0.231	−1.327	−1.133
	$0p\frac{3}{2}$	−0.137	0.419	0.363	0.202	−0.620	−0.538
	$1p\frac{1}{2}$	0.059	−0.429	−0.103	−0.026	0.189	0.046
	$1p\frac{3}{2}$	−0.020	−0.079	−0.135	0.035	0.136	0.231
	$0f\frac{5}{2}$	0.007	−0.064	−0.145	0.013	−0.122	−0.277
	$0f\frac{7}{2}$	0.005	0.020	0.014	−0.002	−0.008	−0.006

TABLE XI. (*Continued*).

ΔE (MeV)			22.34			22.89	
$B(E2)$ (e^2fm^4)			8.45	6.78		9.02	3.77
% of $\Sigma_{cl}^{\Gamma=0}(E2)$			7.2	5.8		7.9	3.3
p	h	S	T (HO)	T (WS)	S	T (HO)	T (WS)
	$0f_{\frac{5}{2}}$	0.005	0.020	0.014	−0.002	−0.008	−0.006
$0f_{\frac{7}{2}}$	$0p_{\frac{3}{2}}$	0.427	3.210	3.205	−0.457	−3.429	−3.424
	$1p_{\frac{3}{2}}$	0.069	−0.660	−1.199	−0.083	0.789	1.433
	$0f_{\frac{5}{2}}$	0.011	−0.042	−0.030	0.005	−0.019	−0.013
	$0f_{\frac{7}{2}}$	0.016	−0.175	−0.284	0.026	−0.285	−0.461
$0g_{\frac{9}{2}}$	$0d_{\frac{5}{2}}$	0.038	0.448	0.345	−0.027	−0.324	−0.249
	$0g_{\frac{9}{2}}$	−0.001	0.023	0.044	−0.000	0.003.	0.006
ΣT (e fm^2)			6.498	5.822		−6.715	−4.344

Table VIII, the PHM approach obtains only 55% and 61% of these classical predictions for the two nuclei if HO wave functions are used, and in the more realistic WS basis, these values are even reduced to 45% and 54% for ^{20}Ne and ^{28}Si, respectively. As for the electric monopole transitions, the lack of strength has to be attributed almost entirely to the truncation of our single particle basis. However, being high up in the continuum, here also the missing orbits would only induce an extremely broad and flat transition strength distribution, which experimentally could hardly be disentangled from the usual background, and their neglect is therefore here equally well justified as for the monopole transitions discussed above.

The theoretical $E2S$-strength distributions obtained for ^{20}Ne and ^{28}Si are displayed in the upper halves of Figs. 7 and 8, respectively. As can be seen, in both nuclei the use of the WS instead of the HO basis yields some modifications of the results. However, although the quadrupole operator has the same radial dependence as the monopole one, the changes are far less drastic here than in case of the monopole transitions. This difference can be easily understood from the fact that the $E0$ transitions are essentially of 1p-particle-0p-hole structure, while in the quadrupole transition amplitudes these terms are dominated by those particle-hole components which involve particle states with higher angular momenta ($0f_{\frac{7}{2}}$, $0f_{\frac{5}{2}}$, $0g_{\frac{9}{2}}$) and the radial wave functions of which—because of the larger centrifugal barrier—are more similar for the two different potentials than those of the 1p levels.

In ^{20}Ne, the most remarkable effects due to the change in the basis wave functions are seen for the transitions to the two states at 22.43 and 22.89 MeV excitation energy, which are analyzed in more detail in Table XI. Similarly as for the monopole transitions, one observes that essential contributions to the decrease of the total transition amplitudes are due to those components which represent a redistribution of the particles inside the pf shell relative to the ground state. So, for example, in both transitions the $0f_{\frac{7}{2}}$-$1p_{\frac{3}{2}}$ and $1p_{\frac{3}{2}}$-$1p_{\frac{3}{2}}$ components are drastically increasing if the WS basis is used, and contribute considerably to the reduction of the total amplitudes.

Similar observations can be made in the case of ^{28}Si (see Table XII). Here the strongest effects are seen for the two transitions to the 26.80 and 28.04 MeV states. Again for both states the change in the pf-pf components yields large contributions to the reduction of the transition amplitudes. However, note that here for the 28.04 MeV transition as well as for the 22.43 MeV transition in ^{20}Ne, a considerable reduction of the matrix elements corresponding to some dominant spectroscopic amplitudes ($0g_{\frac{9}{2}}$-$0d_{\frac{5}{2}}$ in the former, $0f_{\frac{5}{2}}$-$0p_{\frac{1}{2}}$ in the latter case) is observed.

In both nuclei the agreement of the theoretical results with the experimental data is rather satisfying. In ^{28}Si, experiment[17] detects 27(±6)% of the energy weighted isoscalar $E2$ sumrule between 15.5 and 23 MeV. Our calculation obtains in the same energy interval about 26% of the CEWSR for the WS and 28% for the HO basis. In ^{20}Ne the calculations yield 24% (WS) or 34% (HO) between 18 and 28 MeV excitation energy. Here the experiment[15] suggests 35 (+25; −15)% of the CEWSR. Obviously this good agreement should not be overstressed; the theoretical uncertainties (force,

TABLE XII. Same as in Table XI, but for some selected isoscalar electric quadrupole states in ^{28}Si.

			26.80			28.04	
ΔE (MeV)			12.48	5.09		11.62	8.39
$B(E2)$ $(e^2\mathrm{fm}^4)$			7.3	3.0		7.1	5.1
% of $\Sigma_{cl}^{T=0}(E2)$		S	T (HO)	T (WS)	S	T (HO)	T (WS)
$Os_{\frac{1}{2}}$	$Od_{\frac{3}{2}}$	−0.014	−0.048	−0.051	−0.013	−0.043	−0.045
	$Od_{\frac{5}{2}}$	0.010	0.041	0.044	−0.011	−0.047	−0.050
$Op_{\frac{1}{2}}$	$Op_{\frac{3}{2}}$	−0.071	−0.313	−0.312	−0.010	−0.042	−0.042
	$1p_{\frac{3}{2}}$	−0.008	0.023	0.018	−0.001	0.002	0.001
	$Of_{\frac{5}{2}}$	−0.011	−0.068	−0.062	−0.004	−0.027	−0.025
$Op_{\frac{3}{2}}$	$Op_{\frac{1}{2}}$	0.080	−0.350	−0.348	0.010	−0.044	−0.044
	$Op_{\frac{3}{2}}$	0.065	−0.283	−0.287	0.017	−0.074	−0.075
	$1p_{\frac{1}{2}}$	0.007	0.018	0.017	−0.001	−0.001	−0.001
	$1p_{\frac{3}{2}}$	0.007	0.020	0.016	0.001	0.002	0.002
	$Of_{\frac{5}{2}}$	−0.007	−0.023	−0.022	−0.002	−0.008	−0.007
	$of_{\frac{7}{2}}$	−0.012	−0.100	−0.100	−0.005	−0.038	−0.038
$1s_{\frac{1}{2}}$	$Od_{\frac{3}{2}}$	0.049	−0.271	−0.272	0.038	−0.211	−0.212
	$Od_{\frac{5}{2}}$	−0.034	0.228	0.228	0.030	−0.207	−0.207
$Od_{\frac{3}{2}}$	$Os_{\frac{1}{2}}$	0.137	−0.464	−0.493	0.059	−0.200	−0.213
	$1s_{\frac{1}{2}}$	−0.031	−0.170	−0.171	0.037	0.208	0.209
	$Od_{\frac{3}{2}}$	−0.013	0.079	0.079	−0.052	0.317	0.316
	$Od_{\frac{5}{2}}$	0.044	0.178	0.178	0.042	0.168	0.167
$Od_{\frac{5}{2}}$	$Os_{\frac{1}{2}}$	−0.130	−0.543	−0.578	−0.045	−0.187	−0.199
	$1s_{\frac{1}{2}}$	−0.050	0.342	0.342	−0.015	0.102	0.102
	$Od_{\frac{3}{2}}$	−0.027	0.109	0.109	0.024	0.097	0.097
	$Od_{\frac{5}{2}}$	−0.066	0.530	0.528	0.015	0.124	0.124
	$Og_{\frac{9}{2}}$	−0.026	−0.337	−0.309	−0.011	−0.148	−0.136
$1p_{\frac{1}{2}}$	$Op_{\frac{3}{2}}$	0.108	−0.300	−0.276	0.058	−0.160	−0.147
	$1p_{\frac{3}{2}}$	0.015	0.118	0.223	0.007	0.058	0.110
	$Of_{\frac{5}{2}}$	0.009	−0.076	−0.148	−0.003	0.024	0.047
$1p_{\frac{3}{2}}$	$Op_{\frac{1}{2}}$	−0.324	−0.898	−0.695	0.116	0.322	0.249
	$Op_{\frac{3}{2}}$	−0.258	−0.714	−0.573	−0.145	−0.401	−0.322
	$1p_{\frac{1}{2}}$	−0.034	0.269	0.509	0.009	−0.071	−0.135
	$1p_{\frac{3}{2}}$	−0.032	0.255	0.747	−0.021	0.165	0.485
	$Of_{\frac{5}{2}}$	−0.007	0.030	0.062	−0.014	0.061	0.128
	$Of_{\frac{7}{2}}$	−0.019	0.200	0.276	−0.007	0.070	0.096
$Of_{\frac{5}{2}}$	$Op_{\frac{1}{2}}$	−0.465	−2.956	−2.722	0.088	0.556	0.512
	$Op_{\frac{3}{2}}$	0.174	−0.591	−0.557	0.243	−0.824	−0.776
	$1p_{\frac{1}{2}}$	−0.049	0.391	0.766	0.029	−0.231	−0.452
	$1p_{\frac{3}{2}}$	0.020	0.084	0.175	0.021	0.091	0.189
	$Of_{\frac{5}{2}}$	−0.035	0.361	0.588	−0.050	0.520	0.847
	$Of_{\frac{7}{2}}$	0.017	0.071	0.089	0.005	0.022	0.028

TABLE XII. (*Continued*).

ΔE (MeV)			12.48	5.09		28.04 11.62	8.39
$B(E2)(e^2\mathrm{fm}^4)$			7.3	3.0		7.1	5.1
% of $\Sigma^{T=0}_{\mathrm{cl}}(E2)$		S	T (HO)	T (WS)	S	T (HO)	T (WS)
	$Of_{\frac{7}{2}}$	0.017	0.071	0.089	0.005	0.022	0.028
$Of_{\frac{7}{2}}$	$Op_{\frac{3}{2}}$	−0.444	−3.697	−3.703	−0.102	−0.850	−0.852
	$1p_{\frac{3}{2}}$	−0.058	0.606	0.836	0.008	−0.087	−0.121
	$Of_{\frac{5}{2}}$	−0.016	0.066	0.082	−0.013	0.055	0.069
	$Of_{\frac{7}{2}}$	−0.031	0.382	0.428	−0.038	0.460	0.515
$Og_{\frac{9}{2}}$	$Od_{\frac{5}{2}}$	−0.034	−0.450	−0.412	−0.535	−7.042	−6.459
	$Og_{\frac{9}{2}}$	−0.021	0.350	0.709	0.006	−0.103	−0.210
ΣT (e fm^2)			−7.899	−5.045		−7.622	−6.475

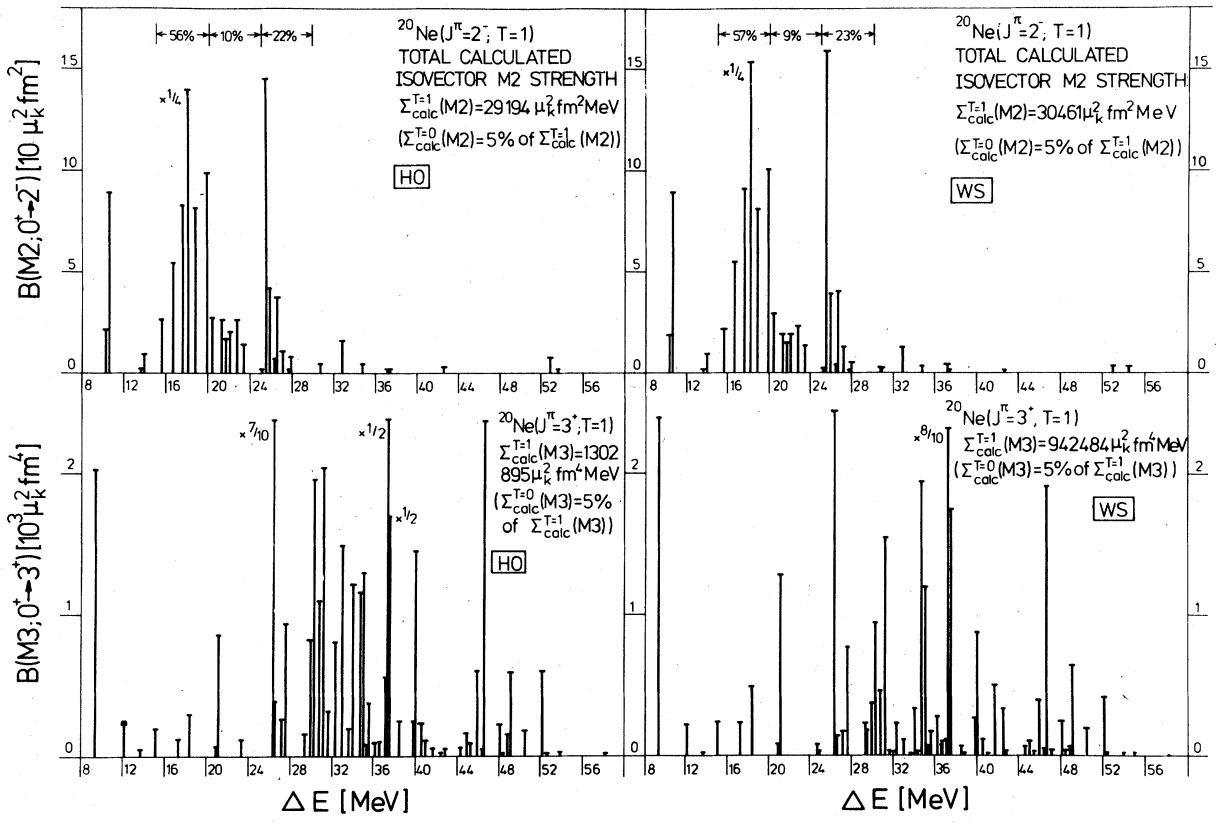

FIG. 9. The isovector magnetic quadrupole and octupole transitions in ^{20}Ne as obtained with the oscillator as well as with the Woods-Saxon basis are given. The strength distribution is here given as a percentage of the calculated sum rules. All $B(M2;0^+\rightarrow 2^-)$ values are in $(10\ \mu_K{}^2\mathrm{fm}^2)$, all $B(M3;\ 0^+\rightarrow 3^+)$ in $(1000\ \mu_K{}^2\mathrm{fm}^4)$.

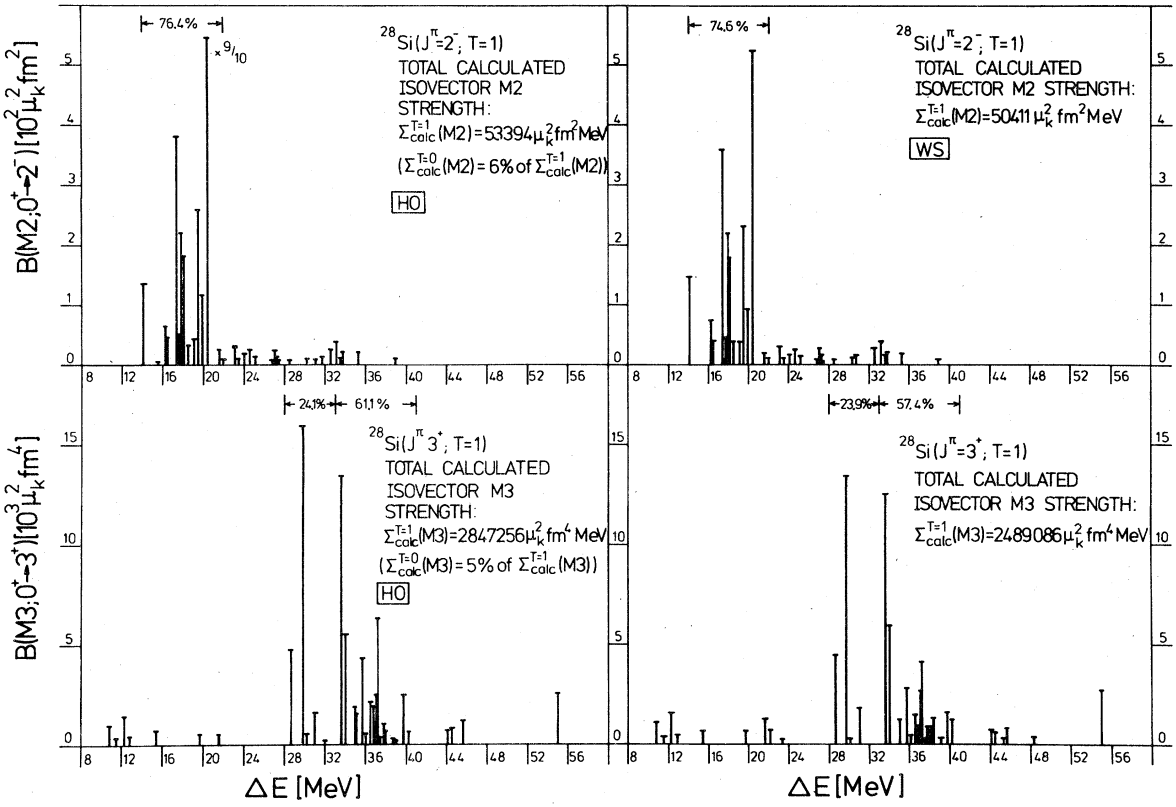

FIG. 10. Same as in Fig. 9 for the nucleus ^{28}Si.

correlation energy, configuration space, etc.) as well as the experimental error bars are still too large to allow definite conclusions. Nevertheless, the agreement gives at least some confidence in the approximations of the PHM approach; even more so since the spreading of the $E2S$ strength in the relevant energy intervals over many states found in the calculations is also compatible with the experimental data.

F. The isovector electric quadrupole transitions ($E2V$)

As already observed in case of the electric monopole mode, for the quadrupole transitions the PHM approach also detects a considerably larger portion of the isovector than of the isoscalar CEWSR of Eq. (30). In ^{20}Ne we obtain 84% (HO) or 66% (WS), in ^{28}Si even 96% (HO) or 83% (WS). Since for isoscalar as well as isovector excitations the same configuration spaces were used and since therefore, as discussed above, a considerable amount of the total strength should be missing also for the isovector quadrupole mode, this result points again to a strong velocity dependence of our Hamiltonian. Unfortunately, as in the monopole case, here also no experimental data for comparison are available, so that the validity of this result cannot be checked. If confirmed, it would indicate the need of a considerably large enhancement factor $\chi(2^+)$ also for the isovector quadrupole CEWSR of Eq. (30).

Not much has to be said about the calculated $E2V$-strength distributions for the two nuclei (lower halves of Figs. 7 and 8 for ^{20}Ne and ^{28}Si, respectively). As expected, in both nuclei the $E2V$ strength is distributed over many levels in a wide energy interval with its center of mass at much higher excitation energy than the main contributions to the $E2S$ strength, and the effects obtained by replacing the HO by the WS basis are of comparable magnitude as those for the isoscalar $E2$ transitions discussed above.

G. The isovector magnetic quadrupole and octupole transitions ($M2V$ and $M3V$)

Owing to the anomalous neutron g factor, not only the magnetic dipole but also the magnetic quadrupole and octupole transitions are essentially of

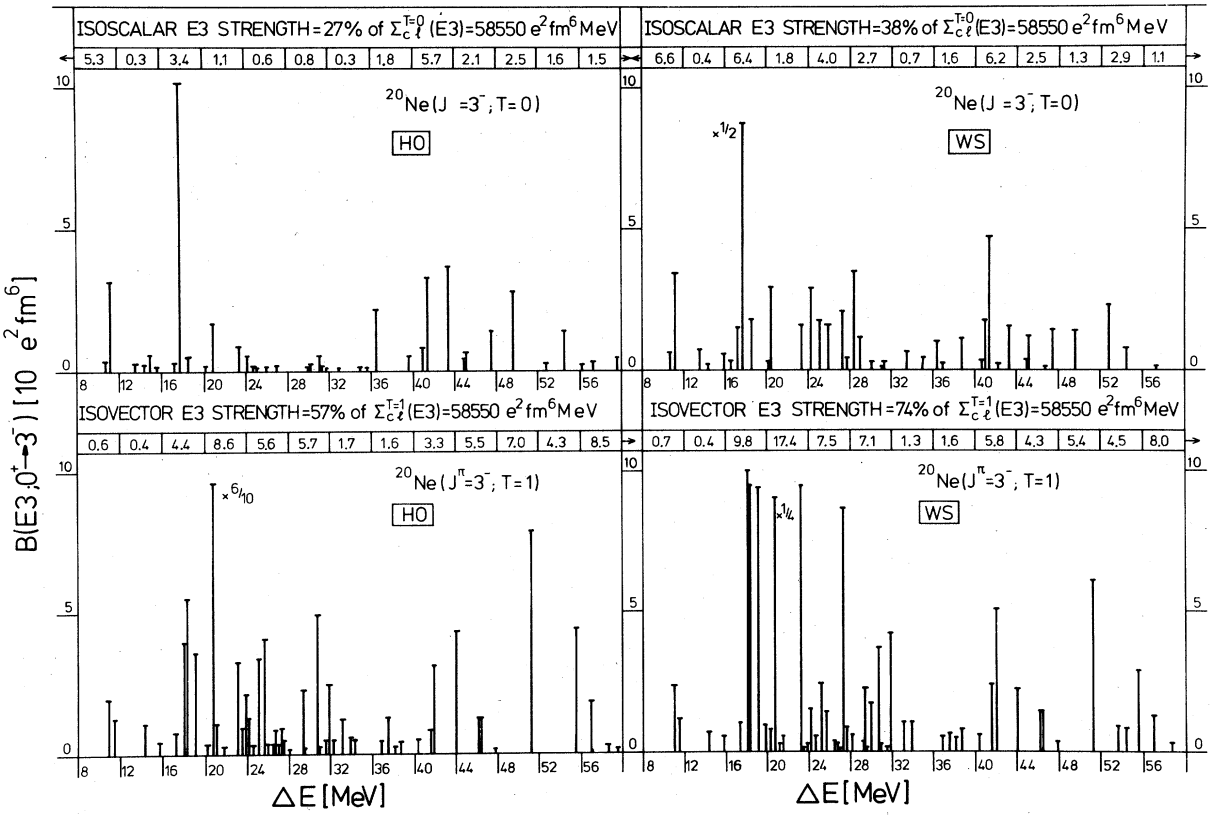

FIG. 11. The isoscalar and isovector electric octupole resonances are displayed. The data obtained with the oscillator basis are compared with those resulting from Woods-Saxon single particle wave functions. Again the strength distributions are given as a percentage of the corresponding classical energy weighted sum rules. All $B(E3;0^+\rightarrow 3^-)$ are in units of $(10\ e^2\,\mathrm{fm}^6)$.

isovector character. As can be seen from Table VIII, the corresponding isoscalar transitions carry in both nuclei less than 6% of the isovector strengths and hence will not be discussed in the present paper.

The $M2V$ and $M3V$ strength distributions for ^{20}Ne and ^{28}Si are presented in Figs. 9 and 10, respectively. As expected from the radial dependence of the corresponding transition operators, the $M2$ values change only slightly if the HO basis is replaced by WS wave functions, while for the $M3V$ mode the changes are of comparable magnitude as those for the electric quadrupole transitions.

In ^{20}Ne, both the $M2V$ as well as the $M3V$ strength is spread over large energy intervals with the main contributions to the latter occuring at higher excitation energies. Here, to our knowledge, no experimental data are available as of yet.

In ^{28}Si the situation looks similar, though here the two modes are both energetically somewhat more concentrated. Here also some experimental data are available.[68] Compared to these data as well as to the results of recent RPA calculations,[68] the PHM approach predicts the main $M2V$ contributions at a few MeV higher excitation energy. However, the ambiguity introduced by the constant energy shift for all the excited states in our calculations and the fact that the measurements were performed only up to 15.5 MeV excitation energy do not allow definite conclusions about this discrepancy.

H. The higher electric multipoles ($E3S$, $E4S$, and $E4V$)

With increasing multipolarity the model space used in the present calculations becomes more and more incomplete: While for the $E0$ and $E2$ transitions essentially only the $2s$, $1d$, and $0g\frac{7}{2}$ orbits are missing in the single particle basis, the description of the total electric octupole ($E3$) strength would require the inclusion of also the 2p, $1f$, and 0h levels, and for the electric hexadecapole ($E4$) transitions in addition even the $3s$, $2d$, $1g$, and $0i$ states should be taken into account.

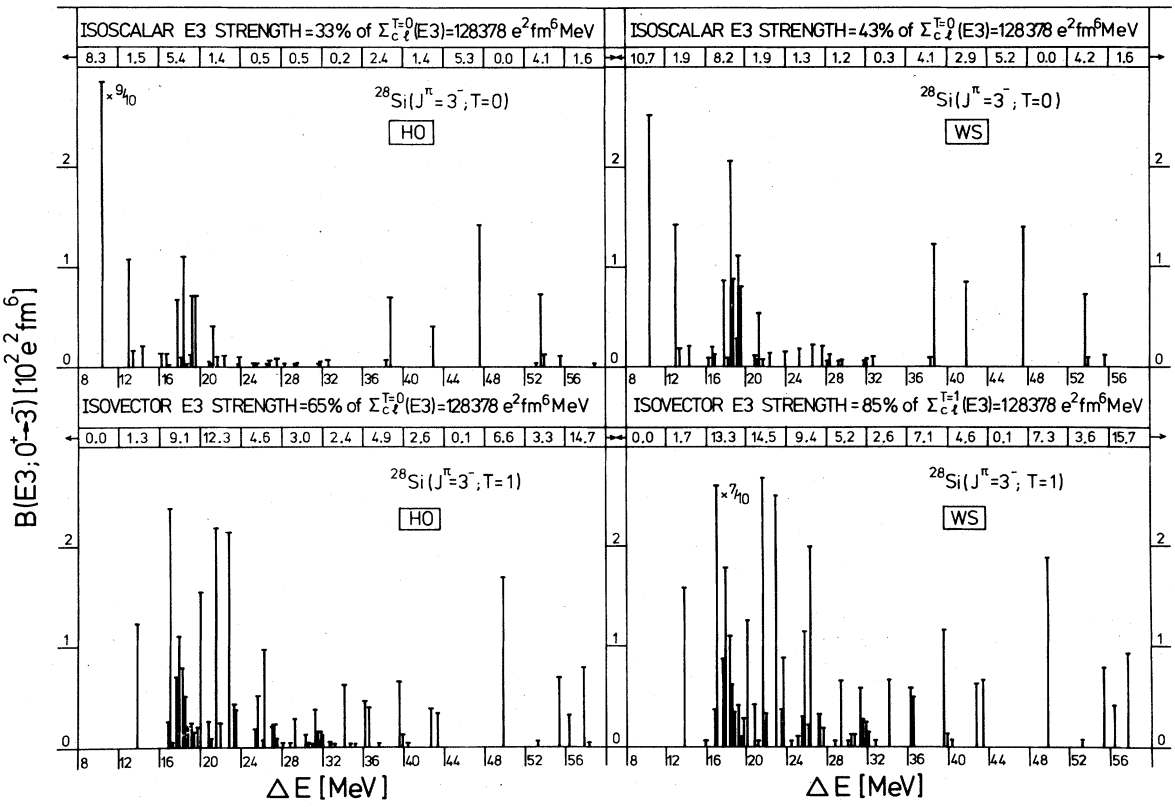

FIG. 12. Same as in Fig. 11, but for ^{28}Si.

However, being even higher up in the continuum than the missing *sdg* orbits, these levels are expected to induce only a broad and rather flat strength continuum at even higher energies than the above discussed neglected $E0$ and $E2$ strength continua. We may therefore hope that at least a large portion of the relevant (because experimentally detectable) $E3$ and $E4$ strengths is still included in our truncated model space, which essentially only contains the $2\hbar\omega$ $E3$ and the $0\hbar\omega$ and $2\hbar\omega$ $E4$ excitations. Nevertheless one should keep in mind that the missing excitations, especially the collective part of them, may still influence the low excited transition in both energy as well as strength. Therefore the calculated $E3$ (Figs. 11 and 12 for ^{20}Ne and ^{28}Si, respectively) and $E4$ strength distributions (Figs. 13 and 14) should be interpreted with some caution. This holds especially for the $E4$ transitions; here, as can be easily seen, due to the r^4 dependence of the corresponding operator, the WS and the HO basis yield drastically different results, and, because of the ambiguity in the WS parameters, it is not obvious whether the real strength distribution should be nearer to the oscillator or the WS prediction. Because of these problems we shall restrict ourselves in the present investigation to only some qualitative conclusions, which may be drawn from the calculated strength distributions.

As far as the isoscalar octupole ($E3S$) transitions are concerned, we obtain in both nuclei, as expected, a few low lying octupole states (some below the energy region displayed in the figures). The rest of the $E3S$ strength in ^{20}Ne as well as in ^{28}Si is spread over many levels and exhausts in none of the indicated 4 MeV intervals more than about 8% of the corresponding CEWSR of Eq. (30), irrespective of whether the HO or the WS representation of the transition operator is used. The experimental detection of $E3S$ resonances by (α,α') measurements, for example, is expected to be rather difficult, since the main $E3S$ contributions are predicted in the region of the $E2S$ resonances and at very high excitation energies. Nevertheless, at least in some energy regions contributions of isoscalar $E3$ strength to the (α,α') angular distributions are expected.

The same holds for the isoscalar hexadecapole ($E4S$) transitions. Also here in both nuclei a large spreading of the total transition strength

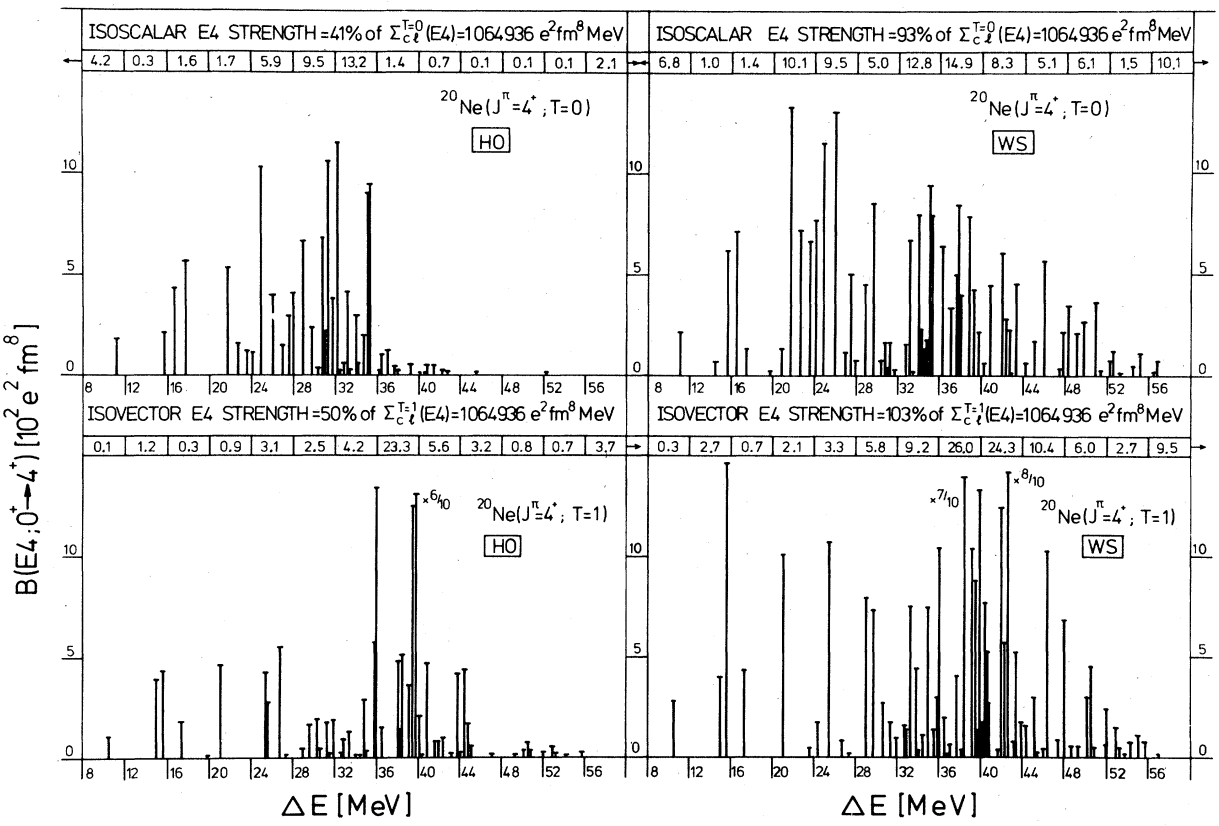

FIG. 13. The isoscalar and isovector electric hexadecapole resonances in ^{20}Ne as obtained by calculations using the oscillator as well as the Woods-Saxon basis. The strength distributions are given as a percentage of the corresponding classical energy weighted sum rules. All $B(E4;0^+\rightarrow 4^+)$ values are given in units of $(100\ e^2\mathrm{fm}^8)$.

over many levels in and above the energy region of the giant quadrupole resonances is obtained and some contributions to the (α,α') angular distributions are to be expected.

About the isovector octupole ($E3V$) and hexadecapole ($E4V$) transitions not much needs to be said. Again, in both nuclei we obtain considerably more isovector than isoscalar strength, a result, which, if confirmed, would point out considerably large enhancement factors $\chi(3^-)$ and $\chi(4^+)$ also for the isovector $E3$ and $E4$ CEWSR's of Eq. (30). The isovector strengths, like the isoscalar ones, are spread over very large energy intervals.

V. SUMMARY

In the present investigation we have tried to describe the structure of the GMR's in the two sd-shell nuclei ^{20}Ne and ^{28}Si on a completely microscopic basis. For this purpose the wave functions for the ground and the excited states in these nuclei were approximated by linear combinations of the angular momentum projected deformed HF vacuum and the angular momentum projected 1p1h excitations with respect to it. The configuration mixing coefficients of this expansion were determined by the diagonalization of the microscopic many nucleon Hamiltonian after restoring the required rotational symmetry from the intrinsic configurations. Such the spin dependence of the configuration mixing was taken into account as well as renormalization effects on the average field, the mixing of components with different total spin projection K on the intrinsic quantization axis was included, and problems with possible linear dependencies in the intrinsic configuration space were avoided. Furthermore, the spurious admixtures due to center of mass excitations were eliminated at least approximately by a separate diagonalization of the center of mass Hamiltonian.

In contrast to Refs. 33, where this angular momentum projected deformed particle hole model (PHM) had been applied to describe the structure of the GMR's in ^{20}Ne as seen via the proton radiative capture reaction on ^{19}F and where, because of the strong selectivity of this reaction, only a

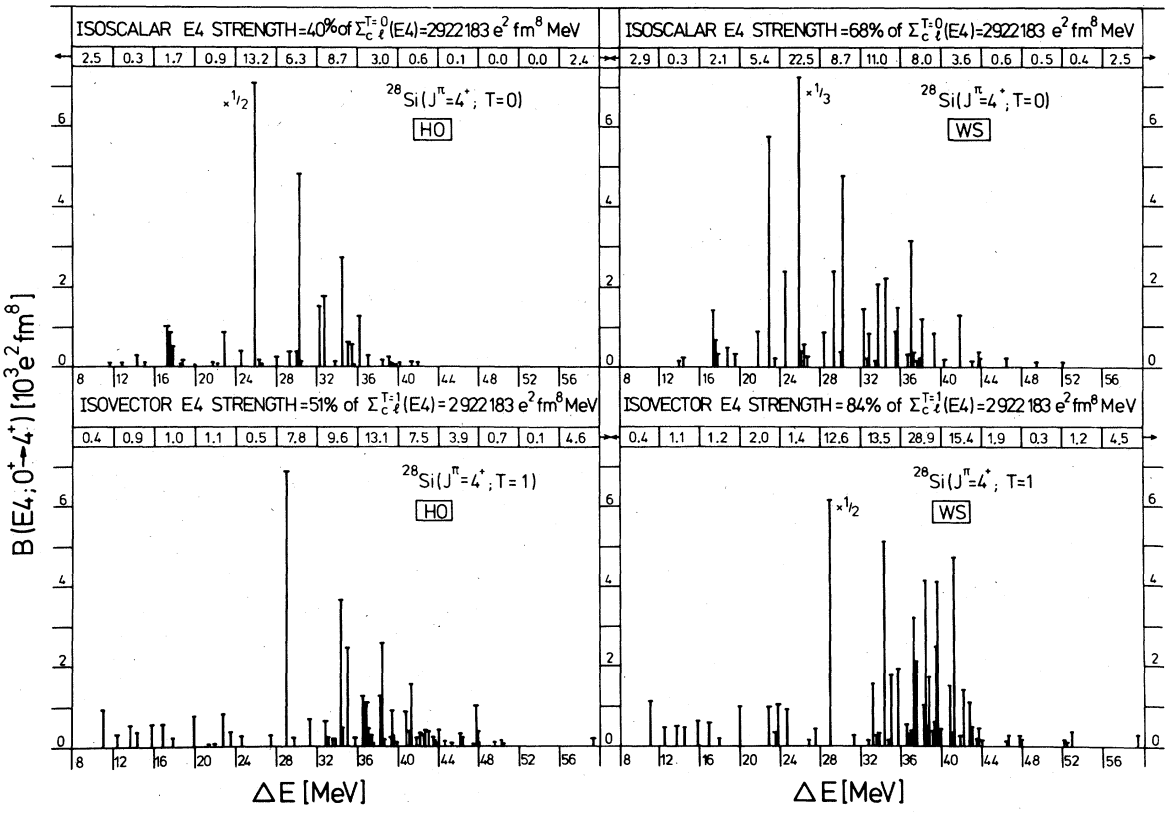

FIG. 14. Same as in Fig. 13 for the nucleus ^{28}Si.

relatively small model space was needed, for the calculations discussed here a rather large single particle basis was used. This enabled us to use a microscopic Brueckner G matrix plus kinetic energy matrix elements as Hamiltonian and such to get rid of the ambiguities induced by the effective forces and single particle energies, which have to be used in small model spaces. Furthermore, because of this large basis no effective charges or g factors had to be introduced.

The only free parameter we used in the present calculation was a constant spin and isospin independent correlation energy, which shifts all the excited states down in energy with respect to the ground state band and is supposed to simulate the net effect of the neglected 2p2h configurations. This is obviously a rather crude approximation and the essential drawback of the PHM approach. In the future a better solution should be found. At the moment, however, nothing better can be done with the present computer facilities.

While energies and wave functions were calculated using an oscillator single particle basis for the calculation of the electromagnetic ground state transitions to the various excited states, Woods-Saxon single particle matrix elements were also used in order to study the influence of more realistic radial wave functions on the transition amplitudes.

The results of the various calculations discussed here may be summarized as follows.

(i). In ^{20}Ne not only the experimental excitation energies of the ground state band are well reproduced, but the sd-shell components of the PHM spectroscopic amplitudes for the 2^+ and 4^+ yrast levels also agree very well with the values obtained by a complete sd-shell SCM calculation[63,66] using an entirely fitted effective Hamiltonian. The same holds also for the structure of the strong isovector magnetic dipole state in this nucleus. In ^{28}Si, the agreement for the ground state band as well as for the magnetic dipole states is less quantitative, but for a microscopic calculation is still rather satisfying.

(ii). In both nuclei the experimental level ordering and relative spacings of the low excited negative parity states are very well described by the PHM approach. On the other hand, a couple of the

experimentally observed low excited positive parity levels are missing in the PHM spectra of the two nuclei. This was to be expected, since most of these states are of many particle-many hole structure with respect to the HF vacuum and hence not included in our configuration spaces.

(iii). Though rather large, for most of the multipolarities the single basis used here is not sufficient to obtain the full classical energy weighted sumrule (EWSR) strength. However, since all the missing particle orbits are high up in the continuum, the corresponding strengths are expected to be extremely spread in energy. Since such a broad strength continuum could experimentally hardly be disentangled from the usual background seen, for example, in (α,α') measurements, for comparison with experiment the configurations taken into account here should be sufficient.

(iv). For all multipolarities we obtain considerably more isovector than isoscalar transition strength. This indicates strong velocity dependent terms in our microscopic Hamiltonian and would indicate, if confirmed, the need of some enhancement factors not only for the electric dipole but also for the other multipole isovector EWSR's.

(v). While for the electric dipole and quadrupole and the magnetic dipole and quadrupole transitions the harmonic oscillator and the Woods-Saxon radial wave functions yield similar results, for the electric monopole, octupole, and hexadecapole and the magnetic octupole transitions drastic redistribution of the transitions strengths are observed if the harmonic oscillator is replaced by the more realistic Woods-Saxon basis. In general the use of Woods-Saxon wave functions increases the spreading of the transition strength distributions and shifts their centers of gravity to higher excitation energies.

(vi). In both nuclei the experimentally observed energy weighted isoscalar electric quadrupole strength is well reproduced by the calculations, and the theoretically obtained spreading of this strength over many levels in the relevant energy intervals is also compatable with the experimental data. On the other hand neither experiment nor the PHM approach obtains, in the two nuclei considered, any energetically concentrated isoscalar electric monopole strength exhausting more than a few percent of the corresponding EWSR.

Taking into account that from a completely microscopic theory like the PHM approach a one to one agreement with the experimental data could not be expected, these results have to be considered rather satisfying. The essential physical structures behind the GMR's in the two nuclei considered seem to be contained in the PHM wave functions. One has therefore good reason to hope that using the PHM results as nuclear structure input in, for example, microscopic (p,γ) calculations like those in Ref. 33 or for a distorted wave Born analysis of inelastic electron or hadron scattering, should also yield satisfying results.

ACKNOWLEDGMENTS

The author thanks Dr. H. Müther for preparing the Brueckner G matrix used in the present calculations and the computer center of the Kernforschungsanlage Jülich, where most of the calculations have been performed. He is furthermore indebted to Dr. A. Faessler, Dr. G. DoDang, Dr. J. Speth, and Dr. J. Dehesa for many helpful discussions.

[1]F. E. Bertrand, Ann. Rev. Nucl. Sci. 26, 457 (1976).
[2]A. van der Woude, Nukleonika 23, 379 (1978).
[3]S. Hanna, Invited paper to the International Conference on Nuclear Physics with Electromagnetic Interactions, 1979, Mainz, West Germany.
[4]G. J. Wagner, Invited paper to the Giant Multipole Resonance Topical Conference, Oak Ridge, Tennessee, 1979.
[5]H. E. Gove, A. E. Litherland, and R. Batchelor, Nucl. Phys. 26, 480 (1961); N. W. Tanner, G. C. Thomas, and E. D. Earle, *ibid.* 52, 29 (1964); R. G. Allas, S. S. Hanna, L. Meyer-Schützmeister, and R. E. Segel, *ibid.* 58, 122 (1964).
[6]P. P. Singh, R. E. Segel, L. Meyer-Schützmeister, S. S. Hanna, and R. G. Allas, Nucl. Phys. 65, 577 (1965).
[7]R. E. Segel, Z. Vager, L. Meyer-Schützmeister, P. P. Singh, and R. G. Allas, Nucl. Phys. A93, 31 (1967).
[8]L. W. Fagg, W. L. Bendel, E. C. Jones, Jr., and S. K. Numrich, Phys. Rev. 187, 1378 (1969).
[9]W. L. Bendel, L. W. Fagg, S. K. Numrich, E. C. Jones, Jr., and H. F. Kaiser, Phys. Rev. C 3, 1821 (1971).
[10]L. W. Fagg, Rev. Mod. Phys. 47, 683 (1975).
[11]D. H. Youngblood, J. M. Moss, C. M. Rozsa, J. D. Bronson, A. D. Bacher, and D. R. Brown, Phys. Rev. C 13, 994 (1976).
[12]D. H. Youngblood, A. D. Bacher, D. R. Brown, J. M. Moss, and C. M. Rozsa, Phys. Rev. C 15, 246 (1977).
[13]K. T. Knöpfle, G. J. Wagner, H. Breuer, M. Rogge, and C. Mayer-Böricke, Phys. Lett. 35, 779 (1975).
[14]A. Kiss, C. Mayer-Böricke, M. Rogge, and P. Turek, Phys. Rev. Lett. 37, 1188 (1976).
[15]K. T. Knöpfle, G. J. Wagner, A. Kiss, M. Rogge, C. Mayer-Böricke, and Th. Bauer, Phys. Lett. 64B, 263 (1976).
[16]M. N. Harakeh, A. R. Arends, M. J. A. DeVoigt, A. G. Drentje, S. Y. van der Werf, and A. van der Woude, Nucl. Phys. A265, 189 (1976).

[17]K. van der Borg, M. N. Harakeh, S. Y. van der Werf, A. van der Woude, and F. E. Bertrand, Phys. Lett. 67B, 405 (1977).
[18]K. T. Knöpfle, G. J. Wagner, P. Paul, H. Breuer, C. Mayer-Böricke, M. Rogge, and P. Turek, Phys. Lett. 74B, 191 (1978).
[19]M. N. Harakeh, K. van der Borg, T. Ishimatsu, H. P. Morsch, A. van der Woude, and F. E. Bertrand, Phys. Rev. Lett. 38, 676 (1977); D. H. Youngblood, C. M. Rozsa, J. M. Moss, D. R. Brown, and J. D. Brown, *ibid.* 39, 1188 (1977); H. P. Morsch, M. Rogge, P. Turek, C. Sükösd, and C. Mayer-Böricke, Phys. Rev. C 20, 1600 (1979).
[20]A. van der Woude, Invited lectures to the topical school on "Nuclear Giant Resonances", University of Granada, Spain, 1979, An. Fisc. 76, 89 (1980).
[21]R. Schneider, A. Richter, A. Schwierczinski, E. Spamer, O. Titze, and W. Knüpfer, Nucl. Phys. A323, 13 (1979).
[22]H. F. Glavish, S. S. Hanna, R. Avida, R. N. Boyd, C. C. Chang, and E. Diener, Phys. Rev. Lett. 28, 766 (1972); J. R. Calarco, S. W. Wissink, M. Sasao, K. Wienhard, and S. S. Hanna, *ibid.* 39, 925 (1977); S. W. Wissink, J. R. Calarco, and S. S. Hanna, Bull. Am. Phys. Soc. 24, 646 (1979).
[23]J. Arvieux, J. P. Albanese, M. Buenerd, D. Lebrun, E. Boschitz, C. H. Q. Ingram, and J. Jansen, Phys. Rev. Lett. 42, 753 (1979).
[24]P. Doll, D. L. Hendrie, J. Mahoney, A. Menchaca-Rocha, D. K. Scott, T. J. M. Symons, K. van Bibber, Y. P. Viyogi, and H. Wiemann, Phys. Rev. Lett. 42, 366 (1979).
[25]G. F. Bertsch and S. F. Tsai, Phys. Rep. C18, 125 (1975); K. F. Liu and G. E. Brown, Nucl. Phys. A265, 385 (1976); J. B. Blaizot, Phys. Lett. 60B, 435 (1976); G. A. Rinker and J. Speth, Nucl. Phys. A306, 360 (1978).
[26]S. Krewald, V. Klemt, J. Speth, and A. Faessler, Nucl. Phys. A281, 166 (1977); S. Krewald, thesis, University of Bonn, 1976 (unpublished).
[27]W. Knüpfer and M. G. Huber, Z. Phys. 276, 99 (1976).
[28]J. S. Dehesa, J. Speth, and A. Faessler, Phys. Rev. Lett. 38, 208 (1977); J. S. Dehesa, S. Krewald, J. Speth, and A. Faessler, Phys. Rev. C 15, 1858 (1977); J. S. Dehesa, thesis, University of Bonn, 1978 (unpublished).
[29]J. Wambach, thesis No. JOL-SPEZ-42, 1979 (unpublished); J. Wambach, V. A. Madsen, G. A. Rinker, and J. Speth, Phys. Rev. Lett. 39, 1443 (1977).
[30]K. W. Schmid and F. Grümmer, Z. Phys. A 292, 15 (1979).
[31]W. Knüpfer, K. Knauss, and M. G. Huber, Phys. Lett. 66B, 305 (1977).
[32]K. W. Schmid and G. DoDang, Z. Phys. A 276, 233 (1976).
[33]K. W. Schmid and G. DoDang, Phys. Lett. 66B, 5 (1977); Phys. Rev. C 15, 1515 (1977); *ibid.* 18, 1003 (1978); K. W. Schmid, Invited lectures at the topical school on "Nuclear Giant Resonances", University of Granada, Spain, 1979, An. Fis. 76, 63 (1980).
[34]P. Froebrich and J. Speth, Proceedings of the International Symposium on Nuclear Physics, Balatonfüred, Hungary, edited by G. Pälla and I. Fodor-Lovas (Budapest, 1975), Vol. 2, p. 571.
[35]B. R. Barett, R. G. L. Hewitt, and R. J. McCarthy, Phys. Rev. C 2, 1199 (1970); *ibid.* 3, 1137 (1971).
[36]T. R. Skyrme, Philos. Mag. 1, 1043 (1956); Nucl. Phys. 9, 615 (1959).
[37]E. Halbert, J. B. McCrory, B. H. Wildenthal, and S. P. Pandhya, Adv. Nucl. Phys. 4, 316 (1971).
[38]P. J. Brussard and P. W. M. Glaudemans, *Shell Model Applications in Nuclear Spectroscopy* (North-Holland, Amsterdam, 1977) and references therein.
[39]I. Kelson, Phys. Rev. 132, 2189 (1963); I. Kelson and C. A. Levinson, *ibid.* 134, B269 (1964); W. H. Bassichis, C. A. Levinson, and I. Kelson, *ibid.* 136, B380 (1964).
[40]G. Ripka, Adv. Nucl. Phys. 1, 183 (1968).
[41]D. J. Thouless, Nucl. Phys. 21, 225 (1960).
[42]R. E. Peierls and J. Yoccoz, Proc. Phys. Soc. (London) A70, 381 (1957); W. H. Bassichis, B. Giraud, and G. Ripka, Phys. Rev. Lett. 15, 930 (1965).
[43]F. Villars, *Many Body Description of Nuclear Structure and Reactions*, Proceedings of the International School of Physics, Enrico Fermi, Course XXXVI, edited by C. Bloch (Academic, New York, 1966).
[44]A. K. Kerman and N. Onishi, Nucl. Phys. A281, 373 (1977); R. A. Sorensen, *ibid.* A281, 475 (1977).
[45]A. R. Edmonds, *Drehimpulse in der Quantenmechanik* (Bibliographisches Institut, Mannheim, 1964).
[46]J. P. Elliot and T. H. R. Skyrme, Proc. Roy. Soc. A323, 561 (1955).
[47]B. Giraud, Nucl. Phys. 71, 373 (1965).
[48]K. W. Schmid and H. Müther, Phys. Rev. C 16, 2050 (1977).
[49]T. Hamada and I. P. Johnston, Nucl. Phys. 34, 382 (1962).
[50]R. K. Tripathi, A. Faessler, and A. D. MacKellar, Phys. Rev. C 8, 129 (1973); R. K. Tripathi, A. Faessler, and H. Müther, *ibid.* 10, 2080 (1974).
[51]T. T. S. Kuo, Nucl. Phys. A103, 71 (1969).
[52]K. W. Schmid, L. Satpathy, and A. Faessler, Z. Phys. 267, 337 (1974).
[53]K. Goeke, A. Faessler, and H. H. Wolter, Nucl. Phys. A183, 352 (1972).
[54]W. Chung and B. H. Wildenthal (unpublished). W. Chung and B. H. Wildenthal, (unpublished).
[55]A. Bohr and B. R. Mottelson, *Nuclear Structure* (Benjamin, Reading, Mass., 1975), Vol. II.
[56]W. Brenig, Adv. Theor. Phys. 1, 59 (1965).
[57]F. Ajzenberg-Selove, Nucl. Phys. A300, 1 (1978); P. M. Endt and C. van der Leun, *ibid.* A310, 96 (1978).
[58]K. W. Schmid (unpublished).
[59]A. Arima, V. Gillet, and J. Ginocchio, Phys. Rev. Lett. 25, 1043 (1970); L. Satpathy, K. W. Schmid, and A. Faessler, *ibid.* 28, 832 (1972); L. Satpathy, K. W. Schmid, S. Krewald, and A. Faessler, Phys. Rev. C 14, 1995 (1976).
[60]B. Castel, I. P. Johnston, B. P. Singh, and J. C. Parikh, Nucl. Phys. A157, 137 (1970).
[61]B. H. Wildenthal, Bull. Am. Phys. Soc. 15, 543 (1970); M. B. Burbank, G. G. Frank, N. E. Davison, G. C. Neilson, S. S. M. Wong, and W. J. McDonald, Nucl. Phys. A119, 184 (1968).
[62]H. E. Gove, University of Rochester Report No. UR-NSRL, 1968.
[63]W. Chung and B. H. Wildenthal, Abstracts of contributed papers to the International Conference on Nuclear Physics with Electromagnetic Interactions, Mainz, West Germany, 1979, No. 1.9.

[64]O. Häusser, T. K. Alexander, A. B. McDonald, G. T. Ewan, and A. E. Litherland, Nucl. Phys. A168, 17 (1971).
[65]P. M. Endt and C. van der Leun, Nucl. Phys. A310, 96 (1978).
[66]W. Chung and B. H. Wildenthal, as in Ref. 63, but No. 1.8.
[67]W. Knüpfer (private communication).
[68]W. Knüpfer, R. Frey, A. Friebel, W. Mettner, D. Meuer, A. Richter, E. Spanner, and O. Titze, Phys. Lett. 77B, 367 (1978).